Spin- and polarization-dependent locally-constant-field-approximation rates for nonlinear Compton and Breit-Wheeler processes

D. Seipt[1,2,3,*] and B. King[4,†]

[1]*Helmholtz Institut Jena, Fröbelstieg 3, 07743 Jena, Germany*

[2]*Gérard Mourou Center for Ultrafast Optical Science, University of Michigan, Ann Arbor, Michigan 48109, USA*

[3]*GSI Helmholtzzentrum für Schwerionenforschung GmbH, Planckstrasse 1, 64291 Darmstadt, Germany*

[4]*Centre for Mathematical Sciences, University of Plymouth, Plymouth PL4 8AA, United Kingdom*

(Received 28 July 2020; accepted 28 September 2020; published 9 November 2020)

In this paper we derive and discuss the completely spin- and photon-polarization-dependent probability rates for nonlinear Compton scattering and nonlinear Breit-Wheeler pair production. The locally constant field approximation, which is essential for applications in plasma-QED simulation codes, is rigorously derived from the strong-field QED matrix elements in the Furry picture for a general plane-wave background field. We discuss important polarization correlation effects in the spectra of both processes. Asymptotic limits for both small and large values of χ are derived and their spin and polarization dependence is discussed.

DOI: 10.1103/PhysRevA.102.052805

I. INTRODUCTION

High-intensity laser experiments have now reached the point of being able to investigate the strong-field regime of quantum electrodynamics (QED). In this novel regime, elementary particles, such as electrons and photons, interact nonperturbatively with extremely strong electromagnetic fields. Recent measurements performed at the RAL-CLF's Gemini laser already hint at the relevance of quantum effects in radiation reaction [1,2]. The next generation of multi-PW high-power lasers [3–7] (for a review, see Ref. [8]) will allow a thorough exploration of this new regime.

The two key strong-field QED processes to be investigated here are the emission of a photon by an electron (or positron), known as *nonlinear Compton scattering* (NLC) [9–11], and the decay of a high-energy photon into an electron-positron pair, known as the *nonlinear Breit-Wheeler* (NBW) process [11,12]. For upcoming strong-field experiments it will be important to know not only the kinematic dependence and the particle spectra, but also the spin and polarization dependency of these processes. The first reason is because polarized high-energy electrons and photons find numerous applications such as nuclear spectroscopy [13] and in being ideal probes for strong-field loop processes such as photon-photon scattering [14–17]. The second is to correctly model the incoherent part of higher-order effects such as the trident process [18–27] (creation of an electron-positron pair from a photon emitted by nonlinear Compton scattering) and double nonlinear Compton scattering [28–32], the polarization of the intermediate particle must be taken into account. This naturally poses the question of how important polarization effects are in the modeling of strong-field electromagnetic cascades [33–41], which are, in general higher than second order in multiplicity. Third, several processes in the extension of strong-field QED to beyond-the-standard-model physics, are sensitive to particular polarization channels, such as axionic nonlinear Compton scattering, which, due to the emission of a pseudoscalar, proceeds only with a spin flip [42–44], and the decay of an axion into an electron-positron pair, which has a preference for the spin of the particles produced [45].

If the electromagnetic background is sufficiently weak, then spin and polarization effects can be studied in perturbative QED. For *linear* Compton scattering this has been done in many works, with Klein and Nishina already studying the effect of photon polarization [46], and others looking at the role of spin and polarization [47–50]. Similarly, the photon polarization dependence of pair production in the collision of two photons was already considered in the seminal work of Breit and Wheeler [51]. However, if the intensity of the background is strong enough that on average more than one photon interacts with an electron, one must consider nonlinear QED processes, typically studied in a *plane-wave background*.

To investigate the relevance of the electron spin in the NLC and NBW processes several authors compared calculations for spin-1/2 Dirac particles with corresponding spin-0 Klein-Gordon particles [52–55]. The effect of the electron being a spin-1/2 particle on the radiated light spectrum was also studied experimentally for the case of strong crystal fields (channeling radiation) [56]. The difference brought by the electron having a spin is that the spin—and its associated magnetic moment—can "flip" during the photon emission which is a quantum effect. In a quantum treatment of radiation emission the photon spectrum has contribution from both the electric charge and from the magnetic moment, and both of these contributions are present even if the incident particles are unpolarized and the final state polarization remains unobserved. The contribution of spin flips to NLC has been studied in a plane-wave pulse in comparison to classical radiation calculations [57,58]. Note the spin can also flip in a laser background due to a nonradiative process [e.g., involv-

*d.seipt@gsi.de

†b.king@plymouth.ac.uk

 ©2020 American Physical Society

ing the (dressed) mass operator], which has been studied in Refs. [59,60]. The combination of radiative and nonradiative spin flipping has been studied semiclassically in a constant magnetic field [61].

In NLC the emitted photon polarization has been studied for an electron in a constant crossed field [18,19,31,62,63], in a monochromatic plane-wave background [64] and recently in a plane-wave pulse [65,66]. The dependence of NLC on the incident electron spin has been calculated in Refs. [67,68] from the one-loop mass operator via the optical theorem (therefore yielding no information about final state polarization properties). The spin-polarization dependence of NLC in a monochromatic plane wave has been studied in Ref. [69] without considering the photon polarization, in Ref. [70] including the photon polarization, and in Ref. [71] in a pulse. In Ref. [72] the electron spin-polarization (averaged over photon polarization) for NLC in a short pulse has been investigated using the density matrix formalism where also the LCFA was calculated. For the case of a constant, homogeneous magnetic field, in which an electron produces (quantum) synchrotron radiation, there have also been several studies for the spin-polarized but photon-unpolarized case [73,74], and all particles polarized [75,76]. In some works special emphasis was placed on radiation by the anomalous spin magnetic moment [74,77]. For a review on spin-polarized particle beams in synchrotrons see, e.g., Ref. [78].

For NBW pair production, the effect of photon polarization (but unobserved spin state of the pair) has been calculated in a monochromatic plane wave [9,18,79,80] and in a constant crossed field [63,67,80]. Similar calculations have been performed also for constant magnetic fields [81] and arbitrary constant electromagnetic fields [82]. The spin of electrons and positrons produced in NBW has also been studied for a monochromatic background [64], and the completely polarized NBW cross sections in a strong linearly and circularly polarized monochromatic plane wave have been calculated in Ref. [83]. Numerical results for a pulsed plane wave were obtained in Ref. [84]. Spin-resolved pair production in a strong field has been calculated also for various different field configurations (and production processes) [85–88].

In the rest frame of an ultrarelativistic charge, an arbitrary strong electromagnetic field "looks" like a crossed field (as shown by, e.g., the Weizsäcker-Williams approximation [89,90]). If the field is sufficiently intense, the length scale on which both NLC and NBW are "formed" is much shorter than the length scale of the shortest inhomogeneity in the laser pulse, namely, its wavelength. Hence, the probabilities can be calculated using a "locally constant" field approximation (LCFA). The significance of strong-field quantum effects can be quantified using the *quantum nonlinearity parameter*, χ, which is defined for electrons and photons as $\chi_{e,\gamma} = |F_{\mu\nu} p^{\nu}_{(e,\gamma)}|/(mE_{\mathrm{cr}})$, where F is the background field strength tensor, $p_{(e,\gamma)}$ is the probe particle momentum, and $E_{\mathrm{cr}} = m^2/|e|$ is the Sauter-Schwinger critical field of QED, with electron mass m and charge $e < 0$. By colliding a high-energy electron beam with an intense laser pulse it is possible to reach the regime where $\chi_e \sim 1$ [91,92]. In the quantum regime the LCFA is valid if $\xi \gg 1$ and $\xi^3/\chi \gg 1$, where $\xi = (m/\kappa^0)(E/E_{\mathrm{cr}})$, E is the field strength, and κ^0 is the frequency of the background. The quantity ξ has the meaning of an inverse Keldysh-type parameter. For practical purposes, and with $\chi \sim 1$, the LCFA can be considered a reasonable approximation for $\xi \gtrsim 10$ [72,93], despite its known limitations [94,95]. Monte Carlo sampling of the LCFA rates [62,95–98] is the central method by which strong-field QED effects are included in high-intensity laser-plasma simulations [39,99–101]. Some polarized LCFA rates have been already implemented in (Monte Carlo) simulation codes to investigate the radiative self-polarization of fermions in different field configurations [102–106] and to model photon polarization effects [63,107], as well as polarized QED cascade formation [41].

A reasonable amount of work has already been performed in investigating the role of polarization and spin in different processes and different electromagnetic backgrounds. Yet a systematic study of all spin and polarization effects of the NLC and NBW processes and a consistent derivation of the LCFA is still lacking. This is achieved in this paper. The results for the completely polarized LCFA rates presented in this paper are suitable for a direct implementation in such numerical frameworks. In the current paper we present compact analytical expressions for the fully polarized NLC and NBW processes. We calculate these processes in a plane-wave pulse, from which the LCFA is derived. We find strong correlations in the spectra between the polarization states of photons and leptons, especially when χ is large. Asymptotic formulas for the fully polarized rates are given for small and large values of the seed particle's quantum parameter, χ. These asymptotic approximations are compared quantitatively to the full LCFA which shows some unexpectedly slow convergence for some particular polarization channels. All polarization channels in each of the processes are visualized for various quantum parameter, and the relative ordering of each channel is explained phenomenologically.

The paper is organized as follows. In Sec. II we introduce the polarization and spin bases and give an overview of the kinematics, crossing symmetry, and general structure of the probabilities. Sections III and IV present the results for NLC and NBW, respectively. Both sections include a presentation of the results for a plane wave and for the LCFA, for which the spin polarized asymptotic scaling for large and small quantum nonlinearity parameter is given. Noteworthy aspects of the results are discussed at the end of each section. In Sec. III we also include an overview of the derivation. In Sec. V the paper is concluded. Appendices A and B contain a detailed derivation of the results for NLC and NBW, respectively. Throughout the paper we employ natural Heaviside-Lorentz units with $\hbar = c = \varepsilon_0 = 1$.

II. POLARIZATION BASIS

We begin by introducing the polarization states of vector and spinor particles that will be appear throughout the calculation and in our final results for the fully polarized nonlinear Compton (NLC) and nonlinear Breit-Wheeler (NBW) rates. We will concentrate on the case of a linearly polarized plane-wave laser pulse of arbitrary temporal shape. We introduce the laser polarization ε^μ and four-wave vector κ^μ, satisfying $\varepsilon\cdot\varepsilon = -1$, $\kappa\cdot\kappa = 0$ and $\varepsilon\cdot\kappa = 0$. The normalized vector potential of the background, $a = eA$ with $e < 0$, de-

pends only on the phase variable $\phi = \kappa\cdot x$, and can be given by $a^\mu(\phi) = m\xi\varepsilon^\mu h(\phi)$, with the classical nonlinearity parameter ξ and an arbitrary shape function $h(\phi)$. In addition, it is useful to define the constant background field tensor $f^{\mu\nu} = \kappa^\mu\varepsilon^\nu - \kappa^\nu\varepsilon^\mu$. Let us also define the magnetic field polarization, β, satisfying $\beta\cdot\beta = -1$, $\beta\cdot\varepsilon = \beta\cdot\kappa = 0$.

The spatial components of the four-vectors $(\varepsilon, \beta, \kappa)$ need to form a right-handed triad. For instance, in the laboratory frame we can choose $\kappa = \omega(1, 0, 0, 1)$, $\varepsilon = (0, 1, 0, 0)$, $\beta = (0, 0, 1, 0)$, where ω is the laser frequency. This ensures that their spatial parts fulfill $\boldsymbol{\kappa}/\omega = \boldsymbol{\epsilon} \times \boldsymbol{\beta}$, i.e., $\boldsymbol{\kappa}$ agrees with the direction of the background field Poynting vector.

A. Photon polarization basis

With the triad of basis vectors $(\varepsilon, \beta, \kappa)$, we can define a (linear) polarization basis for a photon with four-momentum k as

$$\Lambda_1 = \varepsilon - \frac{k\cdot\varepsilon}{k\cdot\kappa}\kappa\,, \qquad \Lambda_2 = \beta - \frac{k\cdot\beta}{k\cdot\kappa}\kappa. \tag{1}$$

By construction the polarization basis vectors fulfill $k\cdot\Lambda_j = 0$ and $\Lambda_i\cdot\Lambda_j = -\delta_{ij}$. An arbitrarily polarized photon (in a pure state) with polarization four-vector ϵ_k can therefore be written as the superposition

$$\epsilon_k = c_1\Lambda_1 + c_2\Lambda_2. \tag{2}$$

We will characterize the photon polarization state using the Stokes parameter $\tau_k = |c_1|^2 - |c_2|^2$, where τ_k is, in general, a real number and $\tau_k \in [-1, 1]$. We note that, if τ_k is chosen to be an integer and $\tau_k \in \{-1, 1\}$, then the photon is produced in an eigenstate of the polarization operator [108], and therefore the polarization will not precess as the photon propagates through the background (reviews of photon-photon scattering can be found in Refs. [109–111]). In this paper, we will consider the case that $\tau_k \in \{-1, 0, 1\}$, where $\tau_k = 0$ indicates an unpolarized photon (in a mixed state), i.e., a polarization average. (For unobserved final state polarization one has to multiply the result by 2.) A photon in the Λ_1 polarization state is polarized parallel to the laser polarization direction in a frame in which k and κ are collinear. A photon in the Λ_2 polarization state is polarized perpendicular to the laser. Hence, we may refer to these photons as $\parallel$- and $\perp$-polarized photons, respectively.

B. Fermions

The spin basis can be chosen in a similar way to the photon polarization basis. It is useful to define a basis that does not precess in the background field. Also, the basis cannot depend on spacetime coordinates, otherwise we would be modifying the spacetime dependency of the Volkov solution, which would not fulfill the Dirac equation anymore. For *linearly polarized backgrounds* in the ε direction our basis for the spin four-vector of an electron with momentum p becomes

$$\zeta_p = \beta - \frac{p\cdot\beta}{p\cdot\kappa}\kappa. \tag{3}$$

Then we see that $\zeta_p\cdot\zeta_p = -1$ and $\zeta_p\cdot p = 0$, but also very usefully: $\zeta_p\cdot\kappa = 0$ and $\zeta_p\cdot\varepsilon = 0$. The choice of this basis vector implies that we are looking specifically at *light-front transverse* polarization, with the spin vectors oriented along the magnetic field in the rest frame of the particle. An important aspect of this choice of the spin-quantization axis is that then $F\cdot\zeta_p = 0$, where F is the background field strength tensor. This fact immediately ensures that the spin vector of the particles does not precess under the Bargman-Michel-Telegdi (BMT) equation [112],

$$\frac{dS^\mu}{d\tau} = \frac{eg_e}{2m}F^{\mu\nu}S_\nu - \frac{e(g_e-2)}{2m}u^\mu\,(u\cdot F\cdot S), \tag{4}$$

where S^μ is a general spin-polarization vector, g_e the electron gyromagnetic ratio, and u^μ its four-velocity. Although ζ_p is defined using the asymptotic momentum, p, we see that we can replace, without loss of generality, p with the "instantaneous" classical kinetic momentum $\pi_p(= mu)$ of the electron in a plane-wave background,

$$\pi_p(\phi) = p - a + \kappa\frac{p\cdot a}{\kappa\cdot p} - \kappa\frac{a\cdot a}{2\kappa\cdot p}, \tag{5}$$

and hence $\zeta_\pi \equiv \zeta_p$.

The choice of the basis above $S^\mu = \zeta^\mu$ therefore ensures that $dS^\mu/d\tau = 0$. Thus, the asymptotic polarization state of the particles agrees with the local values inside the strong background field. This is a special choice of spin basis. In general one could expand the spin vectors in a dreibein: $S^\mu = S_\zeta\zeta_p^\mu + S_\eta\eta_p^\mu + S_\varkappa\varkappa_p^\mu$, where η_p and $\varkappa_p$ are two additional spacelike unit four-vectors perpendicular to p and defined as $\eta_p^\mu = \varepsilon^\mu - \kappa^\mu(p\cdot\varepsilon)/(p\cdot\kappa)$ and $\varkappa_p^\mu = m\kappa^\mu/(\kappa\cdot p) - p^\mu/m$, (noting $F\cdot\eta \neq 0$ and $F\cdot\varkappa \neq 0$). Thus, the BMT equation would imply that a general spin vector precesses. It can be shown that the vectors $(\zeta_p, \eta_p, \varkappa_p)$ are pointing in the direction of the background magnetic field, electric field, and wave vector in the rest frame of the particle [72].

The Dirac bispinors are defined using the spin basis ζ_p, which is manifest in the density matrices [113]:

$$u_{p\sigma_p}\bar{u}_{p\sigma_p} = \tfrac{1}{2}(\not{p} + m)(1 + \sigma_p\gamma^5\not{\zeta}_p), \tag{6}$$

$$v_{p\sigma_p}\bar{v}_{p\sigma_p} = \tfrac{1}{2}(\not{p} - m)(1 + \sigma_p\gamma^5\not{\zeta}_p), \tag{7}$$

where we explicitly introduce the spin index $\sigma_p = \pm 1$ to distinguish states where the spin vector is parallel (spin-$\uparrow$, $\sigma_p = +1$) or antiparallel (spin-$\downarrow$, $\sigma_p = -1$) to ζ_p.

C. General considerations for the polarization-resolved probabilities

Nonlinear Compton scattering (NLC) and nonlinear Breit-Wheeler (NBW) pair production are both $1 \to 2$ first-order strong-field QED processes with one interaction vertex (see Fig. 1). Their corresponding S-matrix elements are related by

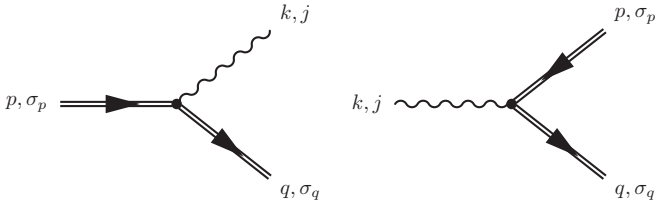

FIG. 1. Feynman diagrams. Left: nonlinear Compton scattering (NLC). Right: nonlinear Breit-Wheeler (NBW) pair production.

crossing invariance. The strong-field QED vertex is an interaction of two "dressed" fermion lines (including the exchange of a number of background laser photons) and one photon line. We preface the detailed calculation of these two processes with some general remarks on the (light-front) kinematics of the processes and the structure of the expressions for the polarization-resolved probabilities.

To have a unified notation for both processes under study, let us denote the incoming momentum as $p_{\rm in}$, the outgoing momentum of the particle under study as $p_{\rm out}$, and the momentum of the outgoing particle we integrate over (i.e., its momentum is not observed, but its polarization state is) as the ancillary momentum q. We orient the coordinate system in such a way that the laser propagates along the *positive* z axis, i.e., $\kappa^+ = 2\omega$ (where light-front momentum components are defined $p^\pm = p^0 \pm p^3$) is the only nonvanishing light-front component of κ^μ. Then, for both processes, NLC and NBW, the light-front momentum conservation can be expressed as

$$p_{\rm in}^- = p_{\rm out}^- + q^-, \qquad \boldsymbol{p}_{\rm in}^\perp = \boldsymbol{p}_{\rm out}^\perp + \boldsymbol{q}^\perp, \tag{8}$$

with $\boldsymbol{p}^\perp = (p^1, p^2)$, and the exchange of "+" momentum between the particles and the background field does not yield a conservation law. In a plane-wave background, one can write the S-matrix element using the four-dimensional light-front δ function $\delta^{(4)}(P + \ell\kappa) = 2\delta(P^+ + \ell\kappa^+)\delta(P^-)\delta^{(2)}(\boldsymbol{P}^\perp) = 2\delta(P^+ + \ell\kappa^+)\delta_{\rm l.f.}(P)$ as

$$S = -ie(2\pi)^4 \int \frac{d\ell}{2\pi}\delta^{(4)}(P + \ell\kappa)\,\mathcal{M}, \tag{9}$$

where $P = p_{\rm in} - p_{\rm out} - q$, and the integral over ℓ takes into account exactly the nonconservation of $+$-momentum. The amplitude $\mathcal{M}$ is specific to each process and contains all the spin and polarization dependence. The phase-space integrated probability for the process under consideration is then given by

$$\mathbb{P} = \frac{1}{2p_{\rm in}^-}\int \widetilde{d^3q}\,\widetilde{d^3p}_{\rm out}\,|S|^2 =: \int d\Gamma\,|S|^2 \tag{10}$$

with the Lorentz-invariant on-shell phase space elements understood in light-front coordinates, i.e., $\widetilde{d^3q} = \frac{dq^- d^2\boldsymbol{q}^\perp}{(2\pi)^2 2q^-}$.

The conservation of three light-front momentum components in Eq. (8) allows one to completely integrate out the ancillary momentum q. The final particle phase space of $\boldsymbol{p}_{\rm out}$ is conveniently parametrized by the normalized light-front momentum transfer s and transverse momentum $\boldsymbol{r}^\perp$:

$$s := \frac{p_{\rm out}^-}{p_{\rm in}^-} = \frac{\kappa\cdot p_{\rm out}}{\kappa\cdot p_{\rm in}}, \qquad \boldsymbol{r}^\perp := \frac{\boldsymbol{p}_{\rm out}^\perp}{ms}. \tag{11}$$

We thus can write the final particle phase space as

$$d\Gamma = dq^- d^2\boldsymbol{q}^\perp \left(\frac{m}{p^-}\right)^2 \frac{s}{1-s}\frac{ds\,d^2\boldsymbol{r}_\perp}{8(2\pi)^6}. \tag{12}$$

Moreover, for the squared S matrix we find

$$|S|^2 = (2\pi)^3 e^2 \left(\frac{2}{\kappa^+}\right)^2 \delta_{\rm l.f.}(P)\,|\mathcal{M}|^2, \tag{13}$$

where we used the normalization $\delta_{\rm l.f.}(0) = \frac{1}{(2\pi)^3}$. Integrating out the ancillary momentum q consumes the δ function and allows the total probability to be expressed as

$$\mathbb{P} = \frac{\alpha}{16\pi^2 m^2 b^2}\int_0^1 \frac{ds\,s}{1-s}\int d^2\boldsymbol{r}_\perp\,|\mathcal{M}|^2, \tag{14}$$

with fine structure constant $\alpha = e^2/4\pi$, and quantum energy parameter $b = p_{\rm in}\cdot\kappa/m^2$. The squared amplitude is given by a double integral over the laser phase, which takes the form

$$|\mathcal{M}|^2 = \int d\phi\,d\phi'\,e^{i\Phi}\,\mathsf{T}_j. \tag{15}$$

Here the integrand is a product of a nonlinearly oscillating factor, the trace of Dirac matrices $\mathsf{T}_j = \Lambda_j^\mu \mathsf{T}_{\mu\nu}\Lambda_j^\nu$ containing the fermion spin structure in $\mathsf{T}_{\mu\nu}$, and photon polarization vectors Λ_j^μ. The specific form of these expressions depends on the considered process. In the following sections, they are evaluated in a linearly polarized plane-wave laser background, first for nonlinear Compton scattering and then for nonlinear Breit-Wheeler pair production. From the general plane-wave results, we then rigorously derive the locally constant field approximation.

III. NONLINEAR COMPTON SCATTERING

This section is devoted to the investigation of fully polarized nonlinear Compton scattering, i.e., the emission of a polarized photon by a spin-polarized electron, where also the spin-polarization after the photon emission is observed. We restrict the discussion to the case of all particles being in polarization eigenstates as discussed above: Initial (final) electrons can be spin-polarized $\sigma_p = \pm 1$ ($\sigma_q = \pm 1$) along the axis ζ_p (ζ_q); photons are emitted in polarization eigenstate Λ_j, $j = 1, 2$.

A. *S* matrix

We begin by recalling the basic properties of Volkov states, which are solutions of the Dirac equation in a plane-wave background,

$$(i\not{\partial} - e\not{A} - m)\Psi_{p\sigma_p}(x) = 0, \tag{16}$$

and, with the normalized vector potential $a = eA$, given by

$$\Psi_{p\sigma_p}(x) = E_p(x)u_{p\sigma_p}, \tag{17}$$

$$E_p(x) = \left(1 + \frac{\not{\kappa}\not{a}}{2p\cdot\kappa}\right)\exp\left(-ip\cdot x - \int d\phi\,\frac{2a\cdot p - a\cdot a}{2\kappa\cdot p}\right), \tag{18}$$

where E_p are the "Ritus matrices," $u_{p\sigma_p}$ are the Dirac bispinors, and $\sigma_p = \pm 1$ means the electrons are asymptotically aligned or antialigned with the spacelike spin-quantization axis ζ_p. Because $\zeta_p = \zeta_\pi$ they remain polarized in that state during the interaction with the laser prior to emitting a photon—and after.

Let us recall that the normalized vector potential a of the background plane wave depends only on the phase variable $\phi = \kappa\cdot x$ and is represented by $a^\mu(\phi) = m\xi\varepsilon^\mu h(\phi)$, where ξ is the classical nonlinearity parameter [62], ε^μ is the polarization vector obeying $\varepsilon\cdot\varepsilon = -1$, and $h(\phi)$ is an arbitrary shape function. Examples of shape functions include $h(\phi) = \cos\phi$, for a linearly polarized infinite plane wave, and

$h(\phi) = \phi$ for a constant crossed field. We now write for the (normalized) field strength tensor $F^{\mu\nu} = m\xi f^{\mu\nu}\dot{h}(\phi)$, where $f^{\mu\nu} = \kappa^\mu\varepsilon^\nu - \kappa^\nu\varepsilon^\mu$ is a constant tensor and $\dot{h}(\phi) = dh/d\phi$.

The S-matrix element for this strong-field QED process (see Fig. 1 left) reads

$$\begin{aligned} &S_{\mathrm{NLC}}(\sigma_p, \sigma_q, j) \\ &\quad = -ie\int d^4x\, \bar{\Psi}_{q\sigma_q}(x)\, \not{A}_j e^{ik\cdot x}\, \Psi_{p\sigma_p}(x) \\ &\quad = -ie(2\pi)^4 \int \frac{d\ell}{2\pi}\delta^{(4)}(p + \ell\kappa - q - k)\, \mathcal{M}_{\mathrm{NLC}} \end{aligned} \tag{19}$$

with the amplitude

$$\mathcal{M}_{\mathrm{NLC}}(\sigma_p, \sigma_q, j) = \Lambda_{j,\mu}\int d\phi\, e^{i\int d\phi \frac{k\cdot\pi_p(\phi)}{\kappa\cdot q}}\, \bar{u}_{q\sigma_q}\mathcal{J}^\mu_{\mathrm{NLC}}(\phi)u_{p\sigma_p}, \tag{20}$$

and the Dirac current which is independent of the polarization properties of all particles

$$\mathcal{J}^\mu_{\mathrm{NLC}}(\phi) = \gamma^\mu + \frac{\not{\kappa}\not{\varepsilon}\gamma^\mu}{2(\kappa\cdot q)} + \frac{\gamma^\mu\not{\varepsilon}\not{\kappa}}{2(\kappa\cdot p)} + \frac{\not{\kappa}\not{\varepsilon}\gamma^\mu\not{\varepsilon}\not{\kappa}}{4(\kappa\cdot p)(\kappa\cdot q)}. \tag{21}$$

B. NLC probability

With the results from Eq. (14) we can write the probability as

$$\begin{aligned} &\mathbb{P}_{\mathrm{NLC},j}(\sigma_p, \sigma_q) \\ &\quad = \frac{\alpha}{16\pi^2 m^2 b_p^2}\int_0^1 \frac{ds\, s}{1-s}\int d^2\boldsymbol{r}_\perp\, |\mathcal{M}_{\mathrm{NLC}}(\sigma_p, \sigma_q, j)|^2, \end{aligned} \tag{22}$$

where the squared amplitude is given by a double phase integral over a dynamic phase factor, which is independent of the particle polarization, multiplied by T_j, which is the Dirac trace $\mathsf{T}^{\mu\nu}$, contracted with the outgoing photon polarization vectors, $\mathsf{T}_j = \Lambda^\mu_j\mathsf{T}_{\mu\nu}(\sigma_p, \sigma_q)\Lambda^\nu_j$. Explicitly,

$$|\mathcal{M}_{\mathrm{NLC}}(\sigma_p, \sigma_q, j)|^2 = \int d\theta\, d\varphi\, e^{i\theta\,\frac{k\cdot\langle\pi_p\rangle}{\kappa\cdot q}}\, \mathsf{T}_j, \tag{23}$$

with $\theta = \phi - \phi'$, $\varphi = (\phi + \phi')/2$, and the floating average defined by

$$\langle\pi_p\rangle = \langle\pi_p\rangle(\varphi, \theta) = \frac{1}{\theta}\int_{\varphi-\theta/2}^{\varphi+\theta/2} d\phi''\, \pi_p(\phi''). \tag{24}$$

The dynamic phase for Compton scattering is given by

$$\theta\frac{k\cdot\langle\pi_p\rangle}{\kappa\cdot q} = \frac{s\theta}{2b_p(1-s)}[\mu + (\boldsymbol{r}^\perp - \langle\boldsymbol{\pi}_p^\perp\rangle/m)^2] \tag{25}$$

with normalized Kibble's mass

$$\mu = 1 + \xi^2\langle h^2\rangle - \xi^2\langle h\rangle^2, \tag{26}$$

energy parameter $b_p = \kappa\cdot p/m^2$, and $s = \kappa\cdot k/\kappa\cdot p$. The spin trace

$$\begin{aligned} \mathsf{T}^{\mu\nu} = \tfrac{1}{4}\mathrm{tr}\,[&(\not{q} + m)(1 + \sigma_q\gamma^5\not{\zeta}_q)\mathcal{J}^\mu(\phi) \\ &\times (\not{p} + m)(1 + \sigma_p\gamma^5\not{\zeta}_p)\bar{\mathcal{J}}^\nu(\phi')] \end{aligned} \tag{27}$$

can be decomposed into four parts: unpolarized (UP), initially polarized (IP, depends only on the initial electron polarization), finally polarized (FP, depends only on the final electron polarization), and polarization correlation (PC, depends on both the initial and final electron polarization). These terms are defined as follows:

$$\mathsf{T}^{\mu\nu}(\sigma_p, \sigma_q) = \mathsf{UP}^{\mu\nu} + \sigma_p\mathsf{IP}^{\mu\nu} + \sigma_q\mathsf{FP}^{\mu\nu} + \sigma_p\sigma_q\mathsf{PC}^{\mu\nu}, \tag{28}$$

with the four contributions

$$\mathsf{UP}^{\mu\nu} \equiv \tfrac{1}{4}\,\mathrm{tr}[(\not{q} + m)\,\mathcal{J}^\mu(\phi)\,(\not{p} + m)\,\bar{\mathcal{J}}^\nu(\phi')], \tag{29}$$

$$\mathsf{FP}^{\mu\nu} \equiv \tfrac{1}{4}\,\mathrm{tr}[(\not{q} + m)\,\gamma^5\not{\zeta}_q\,\mathcal{J}^\mu(\phi)\,(\not{p} + m)\,\bar{\mathcal{J}}^\nu(\phi')], \tag{30}$$

$$\mathsf{IP}^{\mu\nu} \equiv \tfrac{1}{4}\,\mathrm{tr}[(\not{q} + m)\,\mathcal{J}^\mu(\phi)\,(\not{p} + m)\,\gamma^5\not{\zeta}_p\,\bar{\mathcal{J}}^\nu(\phi')], \tag{31}$$

$$\mathsf{PC}^{\mu\nu} \equiv \tfrac{1}{4}\,\mathrm{tr}[(\not{q} + m)\,\gamma^5\not{\zeta}_q\,\mathcal{J}^\mu(\phi)\,(\not{p} + m)\,\gamma^5\not{\zeta}_p\,\bar{\mathcal{J}}^\nu(\phi')], \tag{32}$$

where the NLC current from Eq. (21) and its Dirac adjoint $\bar{\mathcal{J}} = \gamma^0\mathcal{J}^\dagger\gamma^0$ have to be inserted. (FeynCalc [114,115] was used to calculate the traces.) Then the expression for the differential probability can be written as

$$\begin{aligned} \frac{d\mathbb{P}_{\mathrm{NLC},j}}{ds}(\sigma_p, \sigma_q) = \frac{\alpha}{16\pi^2 m^2 b_p^2}\frac{s}{1-s}\int d\varphi\int d\theta\int d^2\boldsymbol{r}_\perp \\ \times\; e^{i\theta\,\frac{k\cdot\langle\pi_p\rangle}{\kappa\cdot q}}[\mathsf{UP}_j + \sigma_p\mathsf{IP}_j + \sigma_q\mathsf{FP}_j + \sigma_p\sigma_q\mathsf{PC}_j], \end{aligned} \tag{33}$$

for photons emitted in a polarization state $j = 1, 2$. Introducing the Stokes parameter τ_k of the emitted photon then yields

$$\frac{d\mathbb{P}}{ds}(\sigma_p, \sigma_q, \tau_k) = \frac{1 + \tau_k}{2}\frac{d\mathbb{P}_1}{ds} + \frac{1 - \tau_k}{2}\frac{d\mathbb{P}_2}{ds}. \tag{34}$$

After evaluating the total of eight different traces, and analytically performing the integration in $\boldsymbol{r}_\perp$, which is Gaussian (the technical details of these steps are giving in Appendix A), and regularizing the resulting expressions (e.g., with an "$i\varepsilon$" prescription [116]), one arrives at the expression for the NLC spectrum in a *plane-wave pulse*:

$$\frac{d\mathbb{P}_{\mathrm{NLC}}}{ds} = -\frac{\alpha}{8\pi b_p}\int d\varphi\int\frac{d\theta}{-i\theta}\, e^{ix_0\theta\mu}\, \mathcal{I}_{\mathrm{NLC}}, \tag{35}$$

$$\begin{aligned} \mathcal{I}_{\mathrm{NLC}} = 1 + \sigma_p\sigma_q + (1-g)\tau_k\sigma_p\sigma_q - \xi^2\Delta h^2\tau_k(1 + g\sigma_p\sigma_q) + \frac{\xi^2\langle\dot{h}\rangle^2\theta^2}{2}(g + \sigma_p\sigma_q) \\ - \frac{i\theta\xi\,\langle\dot{h}\rangle}{2}\Big[s\sigma_p + \frac{s}{1-s}\sigma_q + \tau_k\Big(s\sigma_q + \frac{s}{1-s}\sigma_p\Big)\Big], \end{aligned} \tag{36}$$

where $\Delta h^2 = [h(\phi) - \langle h \rangle][h(\phi') - \langle h \rangle]$, $x_0 = s/[2b_p(1-s)]$, and $g = 1 + s^2/[2(1-s)]$. A numerical evaluation of this expression calls for an additional regularization of that part of $\mathcal{I}_{\rm NLC}$ not containing the laser pulse, i.e., being $\propto \xi^0$. Several methods for this regularization have been discussed in the literature [23,117,118].

The appearance of a preexponential term proportional to $1/\theta^2$ [see, e.g., Eqs. (A21) and (A30)] is known from polarized calculations in a plane wave [66]. In the expression above it has already been treated using integration by parts, giving terms

$$\frac{d(\theta\mu)}{d\theta} = 1 + \xi^2 \Delta h^2 + \frac{\theta^2 \xi^2 \langle \dot{h} \rangle^2}{2}. \tag{37}$$

To acquire the LCFA, and specifically a *local rate*, one performs an expansion of the exponent in Eq. (35) to cubic order in θ and each term in the preexponent to leading order θ. Then the integrals over θ can be performed analytically. Let us define the probability rate $\mathbb{R} = d\mathbb{P}/d\varphi$ as the probability for emission per unit laser phase. Combining (A52) and (A53), the differential NLC rate for all particles polarized is then given by

$$\begin{aligned}\frac{d\mathbb{R}_{\rm NLC}}{ds}&(\sigma_p, \sigma_q, \tau_k) \\ &= -\frac{\alpha}{4b_p}\Big\{[1 + \sigma_p\sigma_q + \tau_k\sigma_p\sigma_q(1-g)]\,\mathrm{Ai}_1(z) \\ &\quad + \Big[s\sigma_p + \frac{s}{1-s}\sigma_q + \tau_k\Big(\frac{s}{1-s}\sigma_p + s\sigma_q\Big)\Big] \\ &\quad \times \frac{\mathrm{Ai}(z)}{\sqrt{z}}\,\mathrm{sgn}\,[\dot{h}(\varphi)] \\ &\quad + \Big(g + \sigma_p\sigma_q + \tau_k\frac{1+g\sigma_p\sigma_q}{2}\Big)\frac{2\mathrm{Ai}'(z)}{z}\Big\}. \end{aligned} \tag{38}$$

The argument of the Airy function $\mathrm{Ai}(\cdot)$, its derivative $\mathrm{Ai}'(\cdot)$ and integral $\mathrm{Ai}_1(z) := \int_z^\infty dx\,\mathrm{Ai}(x)$ is $z = (\frac{s}{\chi_e(\varphi)(1-s)})^{2/3}$ and depends on the local value $\chi_e(\varphi) = \chi_p|\dot{h}(\varphi)|$, where $\chi_p = \xi b_p$. The term $\mathrm{sgn}\,[\dot{h}(\varphi)]$ in the second line of (38) appears because of the oscillating nature of a plane-wave pulse. It shows that this particular term switches its sign each half cycle of the wave together with the direction of the magnetic field. Hence, in an oscillating field with many cycles one can expect that this term averages to zero when integrating the rate over the pulse if the field has a certain symmetry such that integrated over a cycle $\int d\varphi\,\mathrm{sgn}\,[\dot{h}(\varphi)]\mathrm{Ai}(z)/\sqrt{z} \approx 0$. Since z depends only on $|\dot{h}|$ this is the case if the field has some (generalized) parity property $\dot{h}(\phi_0 \pm \phi) \approx -\dot{h}(\phi)$ for some ϕ_0. In order to efficiently radiatively polarize electrons this symmetry needs to be broken, for instance, using an ultrashort subcycle pulse [72] or by a bichromatic (two-color) field [104]. By superimposing a second harmonic with the correct phase, e.g., $\dot{h} = \cos\phi + \cos 2\phi$, the (generalized parity) symmetry is broken and it is impossible to find a ϕ_0 such that $-\dot{h}(\phi) \approx \dot{h}(\phi_0 \pm \phi)$. Similar arguments also hold for NBW pair production [105].

From this expression we can straightforwardly recover literature results for the partially polarized cases. The case for unobserved photon polarization is acquired by setting $\tau_k = 0$ and multiplying the result by 2 (for the sum over the final polarization states)

$$\begin{aligned}\frac{d\mathbb{R}_{\rm NLC}}{ds}&(\sigma_p, \sigma_q, \tau_k = 0) \times 2 \\ &= -\frac{\alpha}{2b_p}\Big[(1 + \sigma_p\sigma_q)\mathrm{Ai}_1(z) + \Big(s\sigma_p + \frac{s}{1-s}\sigma_q\Big) \\ &\quad \times \frac{\mathrm{Ai}(z)}{\sqrt{z}}\,\mathrm{sgn}\,(\dot{h}) + (g + \sigma_p\sigma_q)\frac{2\mathrm{Ai}'(z)}{z}\Big]. \end{aligned} \tag{39}$$

This result agrees with the diagonal elements of the spin-density matrix in Ref. [72].

The rate for unpolarized final state particles, but polarized initial electrons, had been calculated, e.g., by Ritus via the imaginary part of the one-loop electron mass operator [67,68]. We can obtain this from the general expression by setting $\sigma_q = \tau_k = 0$ and multiplying by 4 to take into account the summation over final state particles:

$$\begin{aligned}\frac{d\mathbb{R}_{\rm NLC}}{ds}&(\sigma_p, \sigma_q = 0, \tau_k = 0) \times 4 \\ &= -\frac{\alpha}{b_p}\Big[\mathrm{Ai}_1(z) + s\sigma_p\frac{\mathrm{Ai}(z)}{\sqrt{z}}\,\mathrm{sgn}\,(\dot{h}) + g\frac{2\mathrm{Ai}'(z)}{z}\Big]. \end{aligned} \tag{40}$$

Finally, the case of unpolarized electrons, but polarized photons can be achieved by setting $\sigma_p = \sigma_q = 0$ and multiplying by 2 (which is equivalent to performing an average over incoming spins and a sum over outgoing ones) to achieve

$$\begin{aligned}\frac{d\mathbb{R}_{\rm NLC}}{ds}&(\sigma_p = 0, \sigma_q = 0, \tau_k) \times 2 \\ &= -\frac{\alpha}{2b_p}\Big[\mathrm{Ai}_1(z) + (2g + \tau_k)\frac{\mathrm{Ai}'(z)}{z}\Big], \end{aligned} \tag{41}$$

which agrees with literature results [63].

Finally, the completely unpolarized nonlinear Compton rate is obtained by setting $\sigma_p = \sigma_q = \tau_k = 0$ and multiplying by 4 for the summation over the final electron spin and photon polarization states, yielding [9,10]

$$\begin{aligned}\frac{d\mathbb{R}_{\rm NLC}}{ds}&(\sigma_p = 0, \sigma_q = 0, \tau_k = 0) \times 4 \\ &= -\frac{\alpha}{b_p}\Big[\mathrm{Ai}_1(z) + 2g\frac{\mathrm{Ai}'(z)}{z}\Big]. \end{aligned} \tag{42}$$

We can also make a connection to the expressions calculated by Sokolov and Ternov in a constant and homogeneous magnetic field. Translating the Airy functions into modified Bessel functions of the second kind and setting $\dot{h} = 1$ we get perfect agreement with the expressions from the literature [75].

C. Discussion of the Compton rates

To discuss the relative and absolute weight of the eight different polarization channels, we plot the different NLC emission rates for a constant value of $\chi_e = \chi_p$ in Fig. 2. We can make the following general remarks. For the total yield of photons due to each polarization channel, shown in Fig. 2, we see the channels without a spin flip are much larger than those with a spin flip. The dominant contribution is the nonflip transition when the polarization of the emitted photon is in

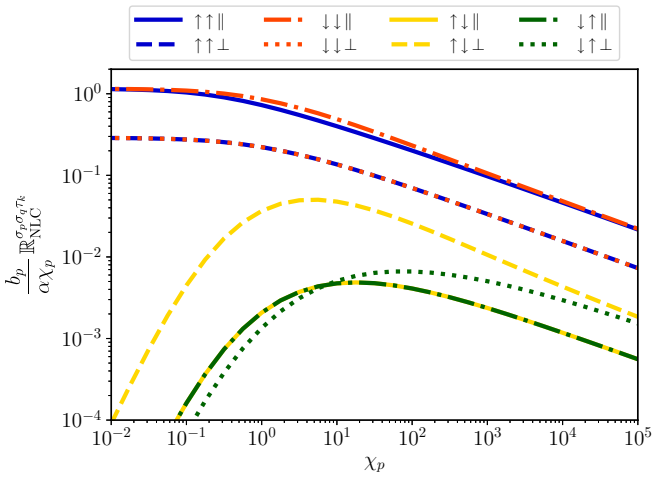

FIG. 2. Polarization-resolved total rates for nonlinear Compton scattering as a function of the electron quantum parameter χ_p.

the ∥ state (which is approximately parallel to the background electric field for a near head-on collision of electron and laser pulse). The nonflip channels with the photon emitted in the ⊥ polarization state are next in the hierarchy of rates. All spin-flip rates are much lower than the nonflip rates. Especially for $\chi_p \ll 1$ they are suppressed by additional powers of χ_p (cf. the discussion of the asymptotic behavior below). The most probable spin-flip channel is the emission of a perpendicularly polarized photon during an ↑ to ↓ transition.

In order to visualize how the differential photon spectrum comprises each polarization channel, in Fig. 3 we select four constant values of χ_p at different orders of magnitude: $\chi_p \in \{0.1, 1, 10, 100\}$. In general, the hierarchy of the various polarization channels can be different in the low-energy infrared part of the spectrum compared to the high-energy UV part of the spectrum. For small $s \to 0$ (where s is the fraction of photon light-front momentum) the rate of spin-flip channels go to zero, showing that the well-known (integrable) infrared divergence of the polarization averaged LCFA rates originates solely in the nonflip channels. For larger values of s the nonflip and spin-flip channels approach each other, and eventually the hierarchy even changes with certain spin-flip channels becoming larger than some nonflip channels. (In other words, it is not just the flip of the spin that determines the hierarchy of rates.) As χ_p is increased, the part of the spectrum where the hierarchy between polarization channels changes moves to larger values of s. [Note that by the conservation law (8) the final state electron normalized light-front momentum is just $1 - s$.]

Also as χ_p increases, a new spectral feature develops in the high-energy part of the spectrum at $s \approx 1$. In Fig. 4 we show the development of this "UV shoulder" in more detail. While the UV shoulder is known to exist and to develop into a pronounced peak approximately located at $s \sim 1 - 4/3\chi_p$ for $\chi_p \gg 1$ [119,120], we see from Fig. 4 that only two of the eight polarization channels are significantly contributing to it, with a strong correlation between the spin-polarization states of all particles for this high-energy feature. This is particularly apparent in the right panel of Fig. 4. For incident down electrons a ∥ photon is emitted and the electron stays in a down state. For incident up electrons, a ⊥ photon is emitted while

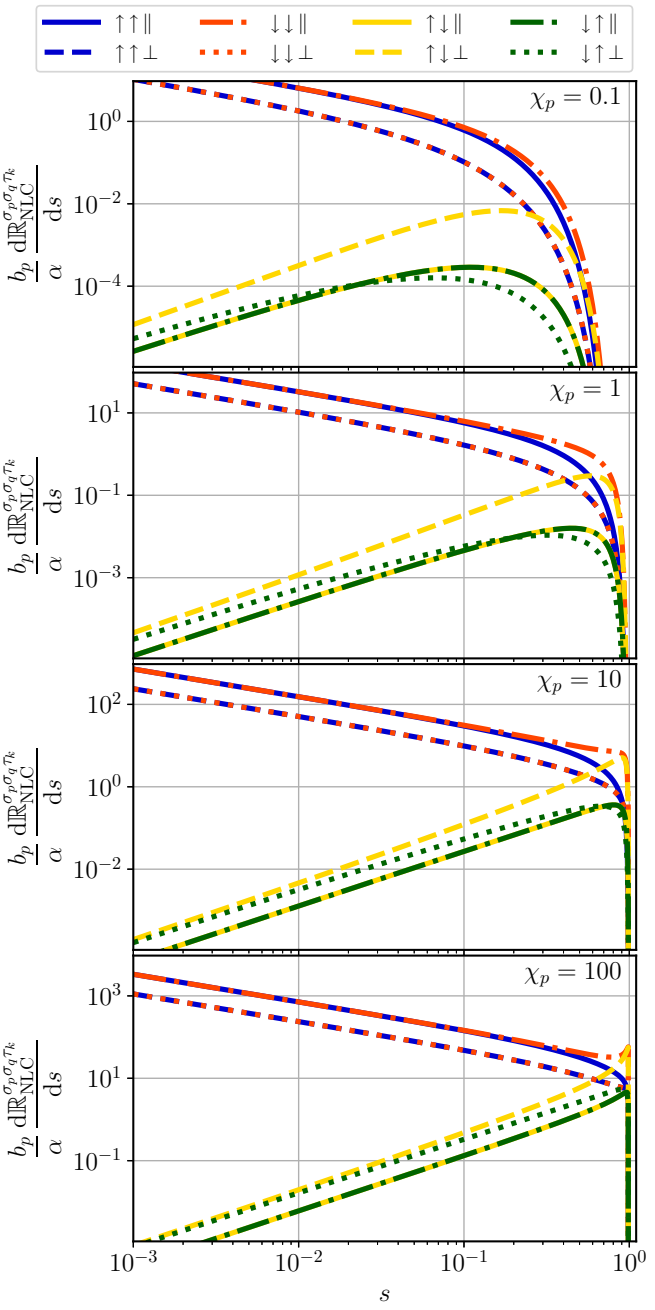

FIG. 3. Plots of the polarization-resolved differential Compton spectra as functions of the normalized photon light-front momentum $s = k^-/p^-$ for four different values of χ_p.

the electron flips to a down state. Thus, by controlling the incident electron polarization one could control the polarization of the generated gamma rays in this high-energy feature of the spectrum. Because the photons have very high energy, almost all of the incident electron energy is transferred to the photon. The existence of the UV shoulder can be clearly seen in calculations of two-step part of second-order processes such as nonlinear trident (NLC followed by NBW) [22,23,25,26], and its existence has been commented on as contributing to free-particle "shower"-type cascades [63].

Although in this section we have thus far focused on the NLC process for *electrons*, analogous arguments apply to

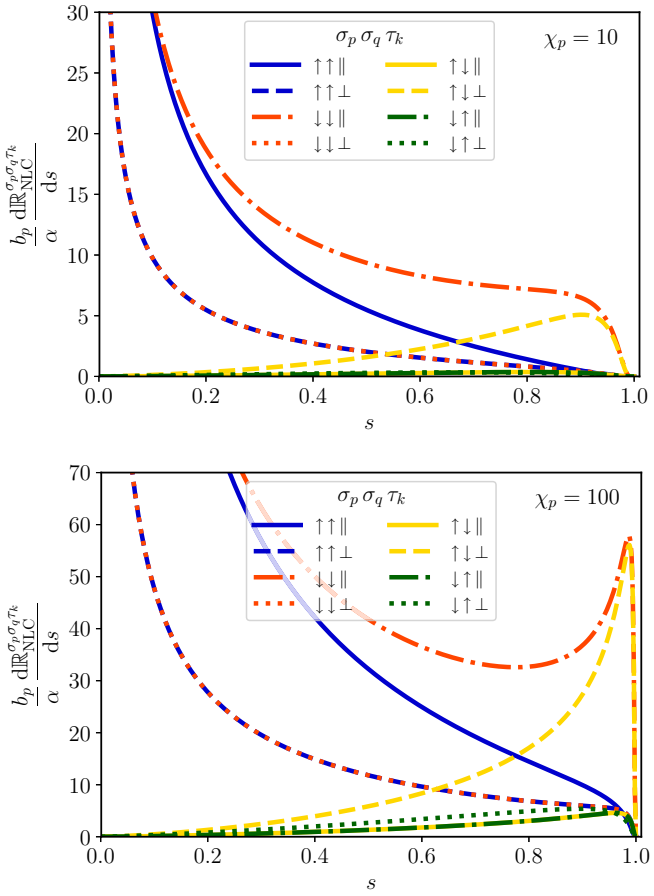

FIG. 4. Differential Compton rate for $\chi_p = 10, 100$ on a linear scale, highlighting the formation of the UV shoulder at $s \simeq 1$ for large χ_p which has a very strong polarization dependence. The electrons emerging from this interaction are strongly down-polarized. There is also a strong correlation between the initial electron polarization and the polarization of the emitted photons in the shoulder.

the NLC process for *positrons*. We note here the necessary changes. First, in the classical kinetic momentum of the electron in a plane wave $\pi_p(\phi)$ from Eq. (5), $a = eA$, where $e < 0$ for an electron. The charge of the positron is positive, $|e|$. Thus, the classical kinetic momentum of a positron differs from that of an electron. The correct expression taking into account the change in the sign of the charge, is given by $-\pi_{-p}(\phi)$.

Moreover, the different sign of the charge for electrons and positrons implies that the vectors of the magnetic moment and spin are parallel in one case and antiparallel in the other case. That means the spin-field interaction has the opposite sign for positrons. Thus, in order to employ the electron NLC rates, Eq. (38), for positrons one also has to make the replacements: $\sigma_p \to -\sigma_p$ and $\sigma_q \to -\sigma_q$. It is evident that neither does this affect the terms in (38) containing the product $\sigma_p\sigma_q$ nor does it affect the spin-averaged rates, Eqs. (41) and (42).

D. Asymptotic limits

For the discussion of the asymptotics of the rate for large and small values of χ_p it is convenient to treat spin flip ($\sigma_q = -\sigma_p$) and nonflip ($\sigma_q = \sigma_p$) separately, as we will find them to have different asymptotic behavior. Here we choose the quantum parameters, $\chi_e = \chi_p$ and $\chi_\gamma = \chi_k$, occurring in the LCFA, to take constant values, which is equivalent to considering the case of a constant crossed field background.

1. $\chi_p \ll 1$

For nonlinear Compton scattering, the χ_k parameter of the emitted photon (which is bounded above by the χ_p parameter of the initial electron) quantifies the recoil when the electron emits a photon. Furthermore, the incoming electron parameter, χ_p, is such that $\chi_p, \chi_k \propto \hbar$. Therefore, the limit of $\chi_p \to 0$ is synonymous with the classical limit. The asymptotic expansion of the total NLC rate $\mathbb{R}_{\mathrm{NLC}}$ for small $\chi_p \ll 1$ can be derived by changing the integration variable from light-front momentum fraction s to z (the argument of the Airy functions) and performing a systematic power series expansion in χ_p, yielding

$$\mathbb{R}_{\mathrm{NLC}}^{\sigma_p,\sigma_p,\tau_k} \sim \frac{\alpha\chi_p}{b_p}\frac{1}{2\sqrt{3}}\Big\{\frac{5}{2}+\frac{3}{2}\tau_k - \Big[\frac{3}{4}\sigma_p(1+\tau_k)+\frac{4+3\tau_k}{\sqrt{3}}\Big]\chi_p + \Big[\frac{5}{2}\sqrt{3}\sigma_p(1+\tau_k)+\frac{5}{48}(75+62\tau_k)\Big]\chi_p^2\Big\}, \quad (43)$$

$$\mathbb{R}_{\mathrm{NLC}}^{\sigma_p,-\sigma_p,\tau_k} \sim \frac{\alpha\chi_p^3}{b_p}\frac{1}{2\sqrt{3}}\Big[\frac{15}{16}-\frac{5}{6}\tau_k+\frac{\sqrt{3}}{2}\sigma_p(1-\tau_k)\Big], \quad (44)$$

as $\chi_p \to 0$. In the nonflip rate, Eq. (43), the leading order is $O(\chi_p)$, and the leading order is independent of the spin state of the incoming electron. A spin splitting (difference between up and down incident electrons) only occurs in the order $O(\chi_p^2)$ and only for $\parallel$ photon polarization, $\tau_k = +1$ (there is no spin splitting at all for the $\perp$ polarization). For the spin-flip rate, the leading term is suppressed at $O(\chi_p^3)$. Here the leading term does show spin splitting, but only for the $\perp$ photon polarization ($\tau_k = -1$). The overall leading order of the photon emission rate agrees with the classical radiation. The suppression of spin effects in the NLC rates for small $\chi_p \ll 1$ is consistent with the fact that spin is a quantum property and spin-sensitive effects should disappear in the classical limit.

2. $\chi_p \gg 1$

The asymptotic expansion of the NLC rate for large $\chi_p \gg 1$ can be calculated by first perturbatively expanding the Airy functions for small argument z. The resulting integrals can be easily performed for the leading order terms stemming from the Ai and Ai$'$ terms, yielding

$$\mathbb{R}_{\mathrm{NLC}}^{\sigma_p,\sigma_p,\tau_k} \sim \frac{\alpha\chi_p^{2/3}}{b_p}\frac{\Gamma\left(\frac{2}{3}\right)}{18\times 3^{1/3}}\Big[13\Big(1+\frac{\tau_k}{2}\Big) - (3\chi_p)^{-1/3}\,\sigma_p(1+\tau_k)\frac{7}{2}\frac{\Gamma\left(\frac{1}{3}\right)}{\Gamma\left(\frac{2}{3}\right)}\Big], \quad (45)$$

$$\mathbb{R}_{\mathrm{NLC}}^{\sigma_p,-\sigma_p,\tau_k} \sim \frac{\alpha\chi_p^{2/3}}{b_p}\frac{\Gamma\left(\frac{2}{3}\right)}{18\times 3^{1/3}}\Big[1-\frac{\tau_k}{2} + (3\chi_p)^{-1/3}\,\sigma_p(1-\tau_k)\frac{5}{2}\frac{\Gamma\left(\frac{1}{3}\right)}{\Gamma\left(\frac{2}{3}\right)}\Big], \quad (46)$$

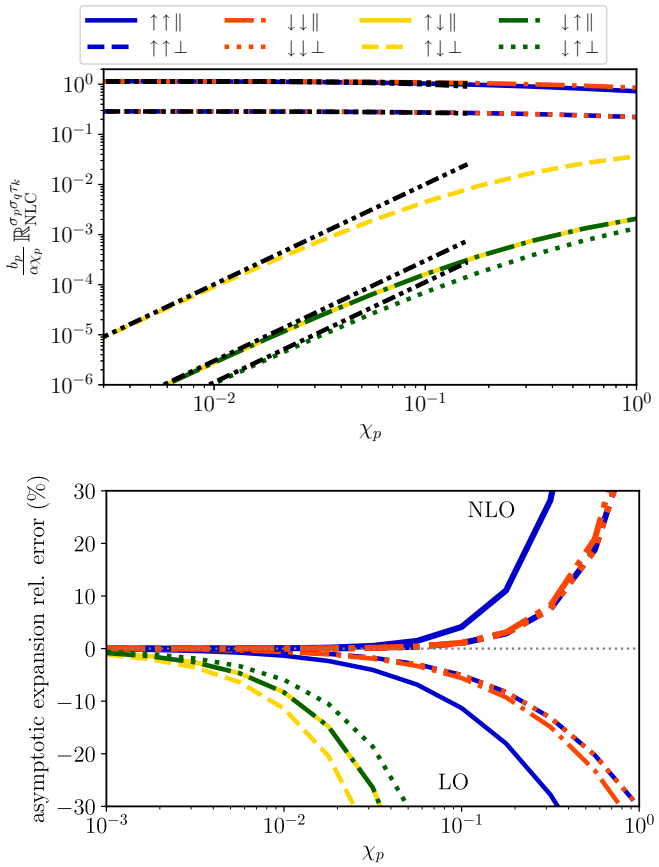

FIG. 5. Comparison of the total nonlinear Compton rates (colored curves according to the legend) with their asymptotic expansions (black dash-double-dotted curves) for $\chi_p \ll 1$ (top) and relative error of the asymptotic expansion (bottom). We compare the leading order (LO) and the next-to-leading order (NLO) for the nonflip rates.

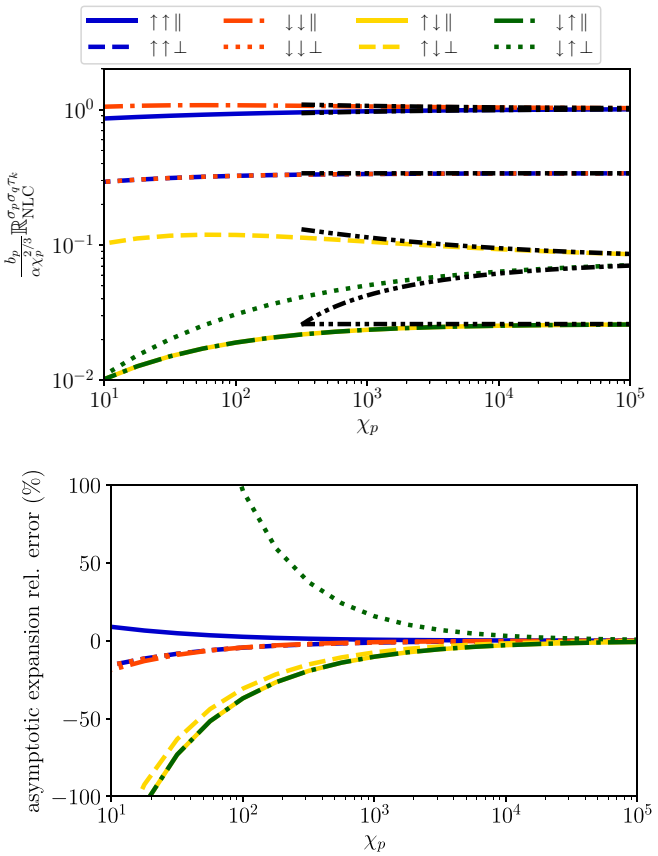

FIG. 6. Comparison of the (scaled) total nonlinear Compton rates with their asymptotic expansions (black dash-double-dotted curves) for $\chi_p \gg 1$ (top) and relative error of the asymptotic expansion (bottom).

as $\chi_p \to \infty$. In this asymptotic limit, for both the spin-flip and nonflip rates the leading order term is $O(\chi_p^{2/3})$ and independent of the spin of the incident electron. Spin dependence occurs only in the next to leading order, which is $O(\chi_p^{1/3})$. This term completely vanishes for unpolarized electrons, where the next nonvanishing term is $O(1)$.

To illustrate the asymptotic scaling of the relations in Eqs. (43)–(46), and their accuracy, the $\chi_p \ll 1$ and $\chi_p \gg 1$ parts of the total yield have been highlighted in Figs. 5 and 6, respectively. As already commented above, we see that in the $\chi_p \to 0$ limit, all spin-flip channels are suppressed by a factor χ_p^2 compared to the nonflip channels. However, we also see that the value of χ_p at which the asymptotic scaling reaches a prescribed level of accuracy, changes, depending on the order of the scaling. To make this manifest, in Fig. 5 (bottom) we plot the relative error of the asymptotic expression, as a function of χ_p. Generally speaking, to arrive at a given accuracy, the asymptotic relations for the spin-flip channels require χ_p to be an order of magnitude more asymptotic, e.g., in the case $\chi_p \ll 1$, an order of magnitude smaller than for the nonflip channels. For example, in the $\chi_p \to 0$ limit, a 10% accuracy is reached by the nonflip relations already at $\chi_p \approx 0.1$, whereas it requires $\chi_p \approx 0.01$ for the same accuracy in the asymptotic relations of the spin-flip channels. Likewise, it is remarkable that the asymptotic expressions in the $\chi_p \to \infty$ limit [see Fig. 6 (bottom)] reach only an accuracy of 10% for $\chi_p \gtrsim 10^3$ for the spin-flip channels. For the spin-flip channel and emission of photon into the $\perp$ polarization, this accuracy is reached at an order of magnitude even larger than this. With present day laser and accelerator technology one can only reach values of $\chi_p \lesssim 10$, and so large χ_p asymptotic expressions can be used only cautiously.

IV. NONLINEAR BREIT-WHEELER PAIR PRODUCTION

A. *S* matrix

To calculate the probability for nonlinear Breit-Wheeler pair production we need to utilize the Volkov state for an (outgoing) positron, which is given by [86,121]

$$\Psi^{(-)}_{p\sigma_p}(x) = E_{-p}(x)\, v_{p\sigma_p}, \tag{47}$$

with the Ritus matrices, Eq. (18), constant positron bispinors $v_{p\sigma_p}$, and where the superscipt "$-$" signifies that the positron Volkov state is a negative energy solution of the Dirac equation (16). Employing (47), the S-matrix element of NBW [see Fig. 1 (right)] can be expressed as follows:

$$\begin{aligned} &S_{\rm NBW}(kj \to p\sigma_p; q\sigma_q) \\ &\quad = \int d^4x\, \bar\Psi_{q\sigma_q}(x)[-ie\not\epsilon_j e^{-ik\cdot x}]\Psi^{(-)}_{p\sigma_p}(x) \\ &\quad = -ie(2\pi)^4 \int \frac{d\ell}{2\pi}\delta^{(4)}(k+\ell\kappa-q-p)\,\mathcal{M}_{\rm NBW}. \end{aligned} \tag{48}$$

We emphasize that p (σ_p) is the four-momentum (spin index) of the created positron and q (σ_q) refers to the electron. The nonlinear Breit-Wheeler amplitude

$$\mathcal{M}_{\rm NBW}(\sigma_p,\sigma_q,j)=\Lambda_{\mu,j}\int d\phi\, e^{-i\int\frac{k\cdot\pi_{-p}}{\kappa\cdot q}d\phi}\,\bar{u}_{q\sigma_q}\mathcal{J}^{\mu}_{\rm NBW}(\phi)v_{p\sigma_p} \tag{49}$$

can be expressed in terms of the current

$$\mathcal{J}^{\mu}_{\rm NBW}(\phi)=\gamma^{\mu}+\left[\frac{\not{a}\not{k}\gamma^{\mu}}{2(\kappa\cdot q)}-\frac{\gamma^{\mu}\not{k}\not{a}}{2(\kappa\cdot p)}\right]h(\phi) -\frac{\not{a}\not{k}\gamma^{\mu}\not{k}\not{a}}{4(\kappa\cdot p)(\kappa\cdot q)}h^2(\phi), \tag{50}$$

where the kinetic momentum of the positron is given by $-\pi_{-p}(\phi)$, with $\pi_p(\phi)$ given in Eq. (5).

The Dirac trace for NBW is

$$\mathsf{T}^{\mu\nu}=\tfrac{1}{4}\mathrm{tr}\,[(\not{q}+m)(1+\sigma_q\gamma^5\not{\zeta}_q)\mathcal{J}^{\mu}(\phi) \times(\not{p}-m)(1+\sigma_p\gamma^5\not{\zeta}_p)\bar{\mathcal{J}}^{\nu}(\phi')] \tag{51}$$

and, using the current from (50), can be decomposed into four parts: unpolarized (UP), electron polarized (EP), positron polarized (PP), and polarization correlation (PC), which are defined as follows:

$$\mathsf{T}^{\mu\nu}(\sigma_p,\sigma_q)=\mathsf{UP}^{\mu\nu}+\sigma_q\mathsf{EP}^{\mu\nu}+\sigma_p\mathsf{PP}^{\mu\nu}+\sigma_p\sigma_q\mathsf{PC}^{\mu\nu}, \tag{52}$$

with the four contributions

$$\mathsf{UP}^{\mu\nu}\equiv\tfrac{1}{4}\,\mathrm{tr}[(\not{q}+m)\,\mathcal{J}^{\mu}(\phi)\,(\not{p}-m)\,\bar{\mathcal{J}}^{\nu}(\phi')], \tag{53}$$

$$\mathsf{EP}^{\mu\nu}\equiv\tfrac{1}{4}\,\mathrm{tr}[(\not{q}+m)\,\gamma^5\not{\zeta}_q\,\mathcal{J}^{\mu}(\phi)\,(\not{p}-m)\,\bar{\mathcal{J}}^{\nu}(\phi')], \tag{54}$$

$$\mathsf{PP}^{\mu\nu}\equiv\tfrac{1}{4}\,\mathrm{tr}[(\not{q}+m)\,\mathcal{J}^{\mu}(\phi)\,(\not{p}-m)\,\gamma^5\not{\zeta}_p\,\bar{\mathcal{J}}^{\nu}(\phi')], \tag{55}$$

$$\mathsf{PC}^{\mu\nu}\equiv\tfrac{1}{4}\,\mathrm{tr}[(\not{q}+m)\,\gamma^5\not{\zeta}_q\,\mathcal{J}^{\mu}(\phi)\,(\not{p}-m)\,\gamma^5\not{\zeta}_p\,\bar{\mathcal{J}}^{\nu}(\phi')]. \tag{56}$$

B. Pair production probability

The evaluation of the traces for NBW pair production is presented in detail in Appendix B. With those, and after performing the integration over the transverse momentum of the outgoing positron, we find the fully polarization-resolved NBW pair production probability in a linearly polarized plane wave of arbitrary shape:

$$\frac{d\mathbb{P}_{\rm NBW}}{ds}=\tfrac{\alpha}{8\pi b_k}\int d\varphi\int_{-\infty}^{\infty}\tfrac{d\theta}{-i\theta}\,e^{i\theta\mu\tilde{x}_0}\,\mathcal{I}_{\rm NBW}, \tag{57}$$

$$\begin{aligned}\mathcal{I}_{\rm NBW}&=1+\sigma_p\sigma_q+\tau_k\sigma_p\sigma_q(1-\tilde{g})\\&\quad+\frac{\xi^2\theta^2\langle\dot{h}\rangle^2}{2}[\tilde{g}+\sigma_p\sigma_q]\\&\quad-\xi^2\Delta h^2\,\tau_k[1+\tilde{g}\sigma_p\sigma_q]\\&\quad-\frac{i\theta\xi\,\langle\dot{h}\rangle}{2}\left[\frac{\sigma_p}{s}-\frac{\sigma_q}{1-s}+\tau_k\left(\frac{\sigma_q}{s}-\frac{\sigma_p}{1-s}\right)\right],\end{aligned} \tag{58}$$

with the positron's light-front momentum fraction $s=p^-/k^-$, $\tilde{g}=1-\frac{1}{2s(1-s)}$, Kibble mass (26) and $\tilde{x}_0$ defined in Eq. (B5).

The initial photon is in a polarization state ϵ characterized by the Stokes parameter $\tau_k=|c_1|^2-|c_2|^2$, where $\epsilon=c_1\Lambda_1+c_2\Lambda_2$. In addition, the definition of Δh^2 given below Eq. (35), as well as the statements about regularization, apply here as well.

Details of the derivation of the LCFA, including the integrals over the phase variable θ are collected in Appendix B. Here we present the final result for the completely polarized NBW pair production rate within the LCFA:

$$\begin{aligned}&\frac{d\mathbb{R}_{\rm NBW}}{ds}(\sigma_p,\sigma_q,\tau_k)\\&=\frac{\alpha}{4b_k}\Bigg\{[1+\sigma_p\sigma_q+\tau_k\sigma_p\sigma_q(1-\tilde{g}]\,\mathrm{Ai}_1(\tilde{z})\\&\quad+\left[\frac{\sigma_p}{s}-\frac{\sigma_q}{1-s}+\tau_k\left(\frac{\sigma_q}{s}-\frac{\sigma_p}{1-s}\right)\right]\frac{\mathrm{Ai}\,(\tilde{z})}{\sqrt{\tilde{z}}}\,\mathrm{sgn}\,(\dot{h})\\&\quad+\left[(\tilde{g}+\sigma_p\sigma_q)+\tau_k\frac{1+\tilde{g}\sigma_p\sigma_q}{2}\right]\frac{2\mathrm{Ai}\,'(\tilde{z})}{\tilde{z}}\Bigg\},\end{aligned} \tag{59}$$

where the argument of the Airy functions is given by $\tilde{z}=[\chi_\gamma(\varphi)s(1-s)]^{-2/3}$. The photon quantum parameter $\chi_\gamma(\varphi)$ again refers to the local value in the field, given by $\chi_\gamma(\varphi)=\chi_k|\dot{h}(\varphi)|$, where $\chi_k=\xi b_k$. The quantum energy parameter $b_k=k\cdot\kappa/m^2$ is related to the center-of-mass energy of the incident photon colliding with the plane-wave laser field. We emphasize again that $s=p\cdot\kappa/k\cdot\kappa$ is the fractional light-front momentum of the *positron* in relation to the light-front momentum of the incident photon. Likewise, σ_p refers to the spin state of the positron, and σ_q to the spin state of the electron.

It is straightforward to recover expressions for totally or partially unpolarized channels. For instance, for the decay of a polarized photon into an unpolarized pair we have to sum over all fermion polarizations, which is equivalent to setting $\sigma_p=\sigma_q=0$ and multiplying the result by 4:

$$\begin{aligned}&\frac{d\mathbb{R}_{\rm NBW}}{ds}(\sigma_p=0,\sigma_q=0,\tau_k)\times4\\&=\frac{\alpha}{b_k}\left[\mathrm{Ai}_1(\tilde{z})+(2\tilde{g}+\tau_k)\frac{\mathrm{Ai}\,'(\tilde{z})}{\tilde{z}}\right].\end{aligned} \tag{60}$$

This agrees with expressions from the literature [63] (sometimes in the literature the Stokes parameter is expressed as $\tau_k=\cos 2\vartheta$, where ϑ is the angle of the photon polarization in relation to the laser polarization, characterized by Λ_1).

To obtain the completely unpolarized NBW rate we have to average Eq. (60) over the incoming photon polarization by setting $\tau_k=0$:

$$\begin{aligned}&\frac{d\mathbb{R}_{\rm NBW}}{ds}(\sigma_p=0,\sigma_q=0,\tau_k=0)\times4\\&=\frac{\alpha}{b_k}\left[\mathrm{Ai}_1(\tilde{z})+2\tilde{g}\frac{\mathrm{Ai}\,'(\tilde{z})}{\tilde{z}}\right].\end{aligned} \tag{61}$$

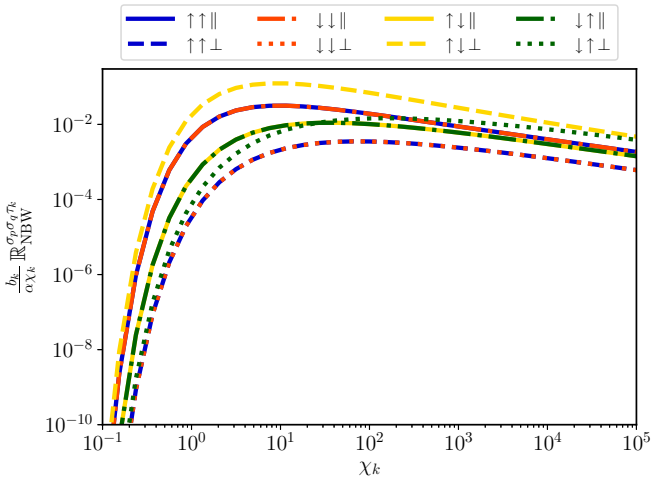

FIG. 7. Scaled total spin-polarization-resolved NBW pair production rates as a function of χ_k.

We can also find the result for the production of a polarized pair by unpolarized photons by just setting $\tau_k = 0$:

$$\frac{d\mathbb{R}_{\mathrm{NBW}}}{ds}(\sigma_p, \sigma_q, \tau_k = 0) = \frac{\alpha}{4b_k}\left\{(1+\sigma_p\sigma_q)\,\mathrm{Ai}_1(\tilde{z}) + [2(\tilde{g}+\sigma_p\sigma_q)]\frac{\mathrm{Ai}'(\tilde{z})}{\tilde{z}} + \left(\frac{\sigma_p}{s} - \frac{\sigma_q}{1-s}\right)\frac{\mathrm{Ai}(\tilde{z})}{\sqrt{\tilde{z}}}\,\mathrm{sgn}(\dot{h})\right\}. \tag{62}$$

C. Discussion of the pair production rates

We illustrate the results for the various polarization channels of NBW pair production in a series of plots, starting with the total rates in Fig. 7. All of the eight channels are strongly suppressed for small χ_k. This is a reflection of the fact that NBW pair production, unlike NLC, is a pure quantum process that must vanish in the classical limit as $\chi_k \to 0$. (See also the detailed discussion of the asymptotic behavior below.) Similar to NLC scattering, the plot of total NBW rates (see Fig. 7) shows a certain hierarchy of the polarization channels which does not change with χ_k, apart from one particular channel where a $\perp$-photon produces a pair with positron spin $\sigma_p = \downarrow$ and electron spin $\sigma_q = \uparrow$. In this channel the pair is produced in its least favourable spin state since the electron spin is aligned parallel to the magnetic field and the positron is aligned antiparallel to the magnetic field. This channel is one of the smallest contributions to the overall rate for small $\chi_k \ll 1$, but is one of the dominant ones for $\chi_k \gg 1$. In general, the most probable channel is the one in which a photon polarized in the $\perp$ state decays into a pair in which the spins are aligned such that their interaction energy with the background magnetic field is minimized, i.e., the electron (positron) is aligned antiparallel (parallel) with the field [76]. This can be seen from the energy in the rest frame of the particle [122], $U_B = -\boldsymbol{\mu}\cdot\boldsymbol{B}$, with $\boldsymbol{\mu} = eg_e\boldsymbol{s}/2m$ (and recalling $e < 0$ for an electron), where $\boldsymbol{s}$ are the spatial components of the spin four-vector $S = \sigma_p\zeta_p$ in the electron rest frame.

In Fig. 8 we plot the light-front momentum spectrum of produced positrons for a range of incoming photon quantum

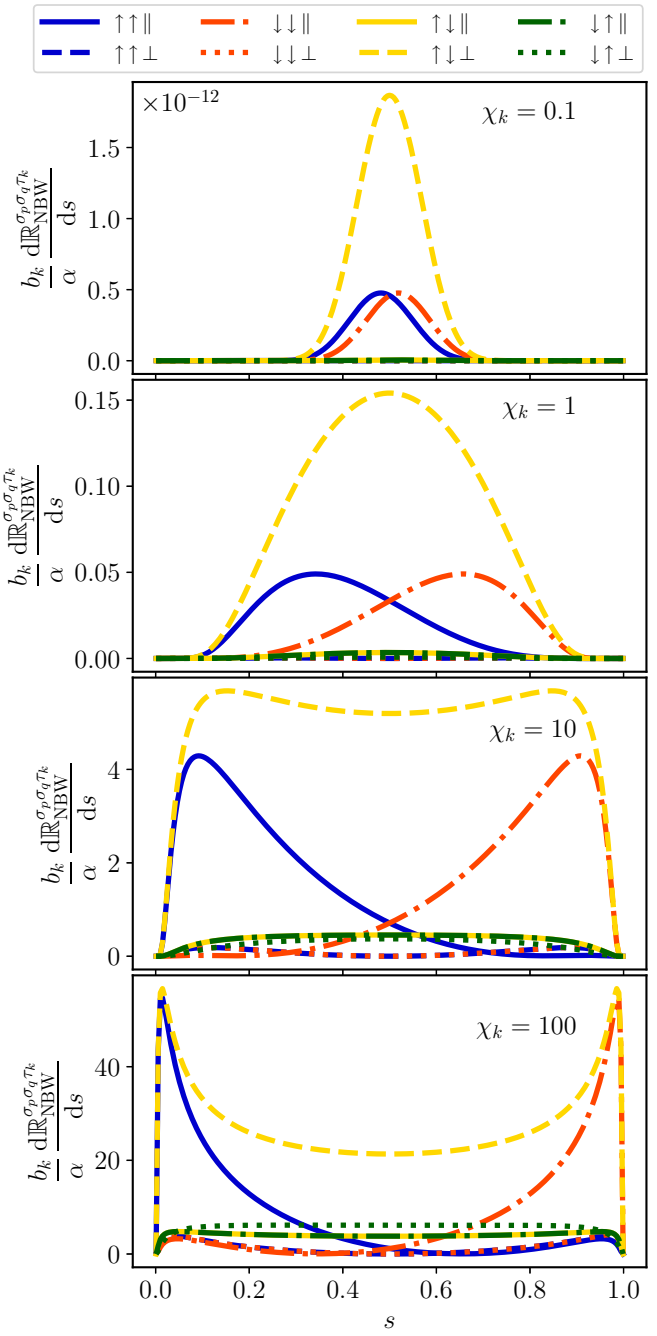

FIG. 8. Spin-polarization-resolved differential NBW pair production rates. Observe how photons of different polarization produce pairs with different symmetry properties. For the largest contribution which comes from $\perp$ photons the spectra are symmetric around $s = 1/2$, and the pair has antiparallel spins with both particles in the desired (lower energy) state. For $\parallel$ photons the pair has preferably parallel spins, with one high-energy particle and one low-energy particle being produced.

parameters, $\chi_k \in \{0.1, 1, 10, 100\}$. It is evident that, especially for smaller values of χ_k, only a few channels are dominant. For increasing χ_k we see new peak structures appear close to $s \sim 0, 1$ which are strongly related to the "UV shoulder" seen in Fig. 4 for NLC [119]. The unpolarized pair production spectrum is symmetric around $s = 1/2$, i.e., symmetric in the exchange of electron and positron $s \leftrightarrow 1 - s$.

In Fig. 8 we clearly see that not all polarization-resolved channels adhere to this symmetry. In particular the channels in which a ∥ photon decays into a pair with parallel spins (i.e., only one of the particles is in its preferred energy state), break the symmetry about $s = 1/2$, meaning that one of the particles is preferably created with a higher momentum than the other one.

D. Asymptotic limits

Here we provide and discuss the asymptotic limits for small and large constant values of χ_k for the spin- and polarization-dependent pair production rates. Here it is convenient to distinguish the case of parallel spins $\sigma_q = \sigma_p$, and antiparallel spins $\sigma_q = -\sigma_p$.

1. $\chi_k \ll 1$

For small χ_k, the asymptotic scaling of the total NBW rate can be calculated by using the fact that for $\chi_k \ll 1$ the argument of the Airy functions $\tilde{z}$ is always large. Performing an asymptotic expansion of the Airy functions for large $\tilde{z}$ yields integrals with a factor $e^{-2\tilde{z}^{3/2}/3}$ which can be treated using Laplace's method [123]. The exponential term turns into the $e^{-8/3\chi_k}$ suppression of the pair production rates which shows up in all combinations of spin and photon polarization and reflects the fact that pair production behaves like a tunneling process in the semiclassical limit for small $\chi_k \ll 1$. Distinguishing the case of parallel spins and antiparallel spins of the generated pair we find

$$\mathbb{R}_{\mathrm{NBW}}^{\sigma_p,\sigma_p,\tau_k} \sim \frac{\alpha}{b_k}\chi_k e^{-\frac{8}{3\chi_k}}\sqrt{\frac{3}{2}}\Big[\frac{1+\tau_k}{2^5} + \frac{13(1+\tau_k)}{3\times 2^{11}}\chi_k + \frac{14\,677 + 11\,221\tau_k}{3^2\times 2^{18}}\chi_k^2\Big], \tag{63}$$

$$\mathbb{R}_{\mathrm{NBW}}^{\sigma_p,-\sigma_p,\tau_k} \sim \frac{\alpha}{b_k}\chi_k e^{-\frac{8}{3\chi_k}}\sqrt{\frac{3}{2}}\Big[\frac{(1+\sigma_p)(1-\tau_k)}{16} + \frac{25-\tau_k+13\sigma_p(1-\tau_k)}{3\times 2^{10}}\chi_k - \frac{707+5005\tau_k-565\sigma_p(1-\tau_k)}{3^2\times 2^{17}}\chi_k^2\Big], \tag{64}$$

as $\chi_k \to 0$.

In Fig. 9 we illustrate the asymptotic limits for small $\chi_k \ll 1$ and scaling of the expressions (63)–(64). Here some interesting observations can be made. In all cases, irrespective of the spin alignment of the pair, the leading order contribution of the NBW rate *explicitly* depends on the incident photon polarization. For all channels there is an overall exponential suppression factor $e^{-8/3\chi_k}$ at small $\chi_k \ll 1$, reflecting the tunneling nature of the NBW pair production process for small χ_k. It is quite interesting, however, that the exact leading order scaling is very much dependent on the specific channel.

For parallel spins, the leading order for ∥ photons ($\tau_k = +1$) is $\propto \chi_k e^{-8/3\chi_k}$, and for ⊥ photons it is much smaller $\propto \chi_k^3 e^{-8/3\chi_k}$ since the first two terms in (63) are proportional to $1+\tau_k$. Moreover, there is no spin-splitting, i.e., the cases ↑↑ and ↓↓ have the same rate. This is in fact true not only for small χ_k as can be seen, for instance, in Fig. 7.

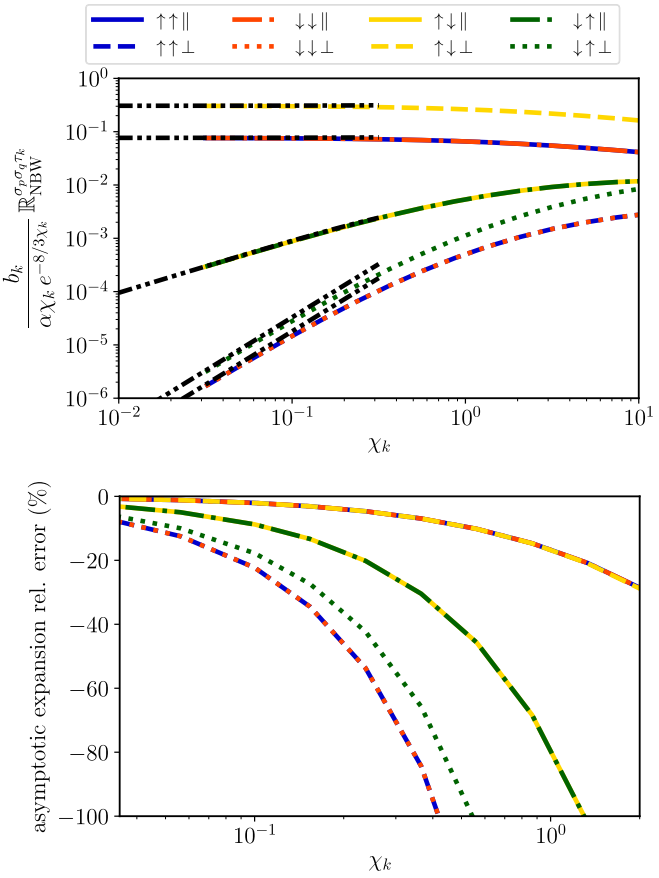

FIG. 9. Asymptotics for spin-polarization-resolved NBW pair production rates for small $\chi_k \ll 1$ (black dash-double-dotted curves) in comparison to the full LCFA rates (top) and relative error of the leading order asymptotic expansion (bottom).

For antiparallel spins the leading order of the rate is even more involved. For ⊥ photons the leading order depends on the spin alignment of the positron. For positrons produced in the favorable ↑ state, the rate is large, $\propto \chi_k e^{-8/3\chi_k}$. However, for positrons produced in the (unfavourable) ↓ state, the leading order is much smaller at $\propto \chi_k^2 e^{-8/3\chi_k}$. This asymptotic result reconfirms the dominance of the ↑↓⊥ channel in Fig. 8 for $\chi_k = 0.01$. For ∥ photons the leading order for antiparallel spins is $\propto \chi_k^2 e^{-8/3\chi_k}$, independent of the spin alignment of the positron.

It is known from the literature that in the limit $\chi_k \ll 1$ the pair production rate of ⊥ photons ($\tau_k = -1$) is twice as large as the rate of ∥ photons [62]. Here we have shown that the former case is dominated by the single spin-polarization channel ↑↓⊥. In contrast, for ∥ photons two equally probable channels contribute. It is also interesting to look at certain ratios of the pair production rates for specific incident photon polarization. For instance, for ∥ photons, $\tau_k = +1$, the probability to generate the pair with antiparallel spins is suppressed as $\mathbb{R}_{\mathrm{NBW}}^{\sigma_p,-\sigma_p,+1}/\mathbb{R}_{\mathrm{NBW}}^{\sigma_p,\sigma_p,+1} \sim \chi_k/8$, which is independent of the value of σ_p. For ⊥ photons, $\tau_k = -1$, we have to distinguish two cases: $\mathbb{R}_{\mathrm{NBW}}^{\sigma_p,\sigma_p,-1}/\mathbb{R}_{\mathrm{NBW}}^{1,-1,-1} \sim 3\chi_k^2/512$ and $\mathbb{R}_{\mathrm{NBW}}^{\sigma_p,\sigma_p,-1}/\mathbb{R}_{\mathrm{NBW}}^{-1,1,-1} \sim 6/11$.

The lower plot in Fig. 9 shows that the asymptotic expressions approximate the NBW rates with a high accuracy only at extremely small values of $\chi_k \ll 1$, and in particular in the interesting range $0.1 < \chi_k < 1$ the relative error can be quite large for some channels. (It should be noted that below $\chi_k < 0.1$ the NBW rate is significantly suppressed because of the exponential factor; see Fig. 7.)

2. $\chi_k \gg 1$

The asymptotic expansion of NBW pair creation for large χ_k is calculated in a similar manner as the corresponding NLC expressions. The asymptotic expressions behave as

$$\mathbb{R}^{\sigma_p,\sigma_p,\tau_k}_{\mathrm{NBW}} \sim \frac{\alpha\chi_k^{2/3}}{b_k}\frac{3\times 3^{2/3}}{14\times 2^{2/3}}\frac{\Gamma\left(\frac{5}{6}\right)}{\Gamma\left(\frac{1}{6}\right)}\left(1+\frac{\tau_k}{2}\right), \tag{65}$$

$$\mathbb{R}^{\sigma_p,-\sigma_p,\tau_k}_{\mathrm{NBW}} \sim \frac{\alpha\chi_k^{2/3}}{b_k}\frac{3^{2/3}}{2\times 2^{2/3}}\frac{\Gamma\left(\frac{5}{6}\right)}{\Gamma\left(\frac{1}{6}\right)}\left[\left(1-\frac{\tau_k}{2}\right) + \chi_k^{-1/3}\,\sigma_p(1-\tau_k)\frac{2^{1/3}}{6\times 3^{1/3}}\frac{\Gamma^2\left(\frac{1}{6}\right)}{\Gamma^2\left(\frac{5}{6}\right)}\right], \tag{66}$$

as $\chi_k \to \infty$.

Here the scalings with χ_k are in principle the same as for NLC, just the numerical factors are different. The main difference is that there is no term at order $\chi_k^{1/3}$ for the case of parallel spins. The asymptotic expressions for large $\chi_k \gg 1$, Eqs. (65)–(66) are plotted in Fig. 10 (top) and the corresponding relative error (bottom).

The asymptotic plots of the total yield in Figs. 9 and 10 also display the behavior of the "anomalous" channel, $\downarrow\uparrow\perp$. First, it is the only polarization channel to cross the others, being as improbable as the least probable channel in the $\chi_k \to 0$ limit since the first two terms in Eq. (64) vanish, but increasing in importance as χ_k is increased until the $\chi_k \to \infty$ limit where it is as probable as the most probable channel. It is remarkable that even by χ_k as large as $O(10^5)$, it has not yet reached its asymptotic value. This fact becomes particularly clear by looking at the relative error of the asymptotic expansions in the bottom panels of Figs. 9 and 10. We notice the same behavior as in the NLC case, that the leading order asymptotic expressions are more accurate already at less extreme asymptotic parameter, whereas the less probable channels require much larger (smaller) values of χ_k to reach a given accuracy in the $\chi_k \to \infty$ ($\chi_k \to 0$) limits.

V. SUMMARY

In this paper we have given a comprehensive overview of the rates of two of the most important strong-field QED processes with the polarization of all particles taken into account. We introduced expressions for fully polarized nonlinear Compton scattering (NLC) and nonlinear Breit-Wheeler pair-creation (NBW) in a general plane-wave background and derived concise formulas for the fully polarized locally constant field approximation (LCFA) of each process. The asymptotic scaling for each process and all of the eight polarization channels has been derived and presented in succinct expressions, and this scaling has been benchmarked against the full LCFA result. Although some of these results exist in other works in the literature, this is, to the best of our knowledge, the first complete presentation and in-depth analysis of all polarization channels together. In doing so, we have been able to resolve particle spectra by polarization channel, and have demonstrated that certain spectral features (such as the appearance of a "UV shoulder or peak" at large quantum parameter), are particular to specific polarization channels. We have also identified "anomalous" channels that change in relative importance as the corresponding quantum parameter is increased.

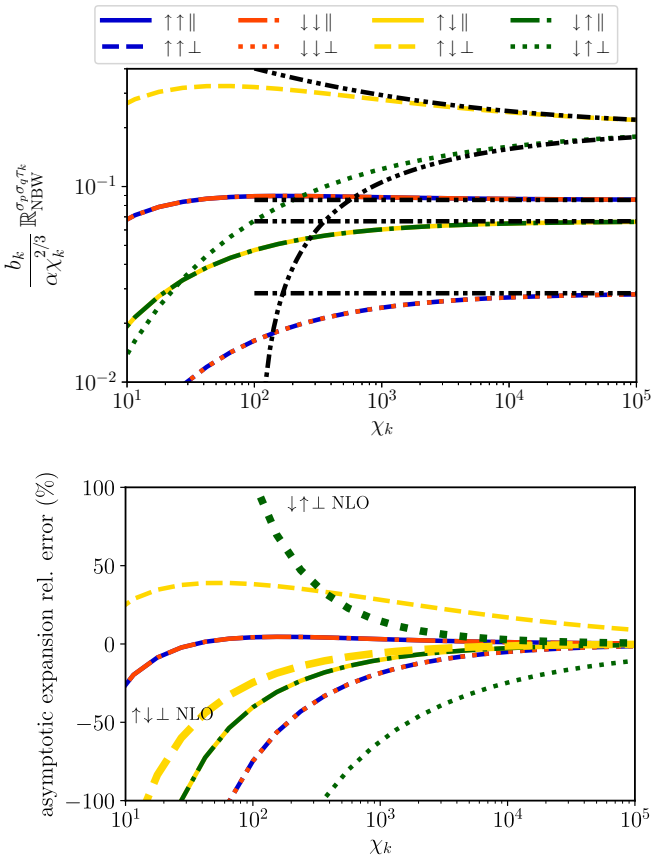

FIG. 10. Asymptotics for spin-polarization-resolved pair production rates (black dash-double-dotted curves) in comparison to the full LCFA for large $\chi_k \gg 1$ (top) and relative error of the asymptotic expansion (bottom) at leading order, except when denoted as NLO.

We note from our results that some polarization channels do not reach their large-χ asymptotic scaling until $\chi \gtrsim O(10^3)$. The Narozhny-Ritus conjecture predicts a breakdown of the QED perturbation expansion in dressed vertices when $\alpha\chi^{2/3} \sim O(1)$ [124–127], i.e., $\chi \sim O(10^3)$. Furthermore, polarized one-vertex tree-level processes such as in NLC and NBW are necessary in order to correctly factorise higher-order tree-level processes in this perturbation expansion. Therefore it is likely that the resolution of the Narozhny-Ritus conjecture has implications for the relative importance of polarization channels in NLC and NBW at large χ.

All our results have been expressed in a polarization basis that respects the symmetry of the background field. However, depending on how polarization is measured in experiment, the polarization of any "detector" must be borne in mind. For example, a measurement of high energy photon polarization has been suggested, which uses the polarization-dependent

probabilities for Bethe-Heitler pair creation in a Coulomb field [16,128]. Therefore it is the projection of our results onto the natural basis of the Bethe-Heitler polarimeter, which will play a role in any detection. The measurement of the spin-polarization of high-energy electrons is often performed using Møller polarimeters [129,130], which, however, are most sensitive to longitudinal polarization, or Compton polarimeters [131,132] which exploit angular asymmetries in the scattering spectra of *linear* Compton scattering. Some authors also propose to use nonlinear QED processes themselves for polarimetry applications [133,134]. A review for existing and future electron beam polarimetry can be found in Ref. [135].

Even if the polarization of the incoming or outgoing particle is not measured, then the LCFA rates for the eight different polarization channels we have presented are still relevant for higher-order processes. The correct factorization of higher-order processes require a consistent polarization of intermediate particles (propagators) between vertices. In this way, the polarized LCFA rates presented here can be directly employed in numerical simulations of electromagnetic cascades in intense background fields [41].

ACKNOWLEDGMENT

B.K. acknowledges support from the EPSRC, Grant No. EP/S010319/1.

APPENDIX A: DETAILS OF THE CALCULATION OF THE LCFA FOR NONLINEAR COMPTON

We start by giving some important kinematic definitions:

$$s \equiv \frac{\kappa\cdot k}{\kappa\cdot p}, \tag{A1}$$

$$g = 1 + \frac{s^2}{2(1-s)}. \tag{A2}$$

With help of the auxiliary variable L, we can find some useful kinematic relations for the incident electron momentum p, outgoing electron momentum q and emitted photon momentum k,

$$p\cdot q = m^2 + Ls\,\kappa\cdot p, \tag{A3}$$

$$q\cdot k = L\,\kappa\cdot p, \tag{A4}$$

$$p\cdot k = L(1-s)\,\kappa\cdot p, \tag{A5}$$

where

$$L = \frac{s}{2\kappa\cdot p(1-s)}\left[m^2+\frac{X_\varepsilon^2+X_\beta^2}{s^2}\right] = x_0\left[1+\left(\frac{\boldsymbol{p}_\perp}{m}-\boldsymbol{r}_\perp\right)^2\right], \tag{A6}$$

and we introduced the normalized transverse momentum of the photon, $\boldsymbol{r}_\perp = \boldsymbol{k}_\perp/ms$, and the auxiliary variables $X_\varepsilon = k\cdot\varepsilon - sp\cdot\varepsilon$ and $X_\beta = k\cdot\beta - sp\cdot\beta$. In addition,

$$x_0 = \frac{s}{2b_p(1-s)}, \tag{A7}$$

with $b_p = \kappa\cdot p/m^2$.

1. NLC traces

Here we list the expressions for all 8 Dirac traces for nonlinear Compton scattering, Eqs. (29)–(32). They are evaluated using FEYNCALC [114,115]. Here we use the short-hand notation h' for $h(\phi')$ and h for $h(\phi)$, and also write $h-h' = \int_{\phi'}^{\phi}\dot{h}(\varphi)d\varphi = \theta\langle\dot{h}\rangle$, with $\theta = \phi-\phi'$ being the laser phase difference between the NLC amplitude and its complex conjugate.

$$\mathsf{UP}_1 = q\cdot p - m^2 - \frac{m^2\xi^2(s-2)^2}{2(s-1)}hh' + \frac{m\xi(s-2)^2}{2(s-1)s}X_\varepsilon(h+h') + \frac{2X_\varepsilon^2}{s^2}, \tag{A8}$$

$$\mathsf{UP}_2 = -q\cdot p - m^2 + 2\frac{k\cdot q}{s} + 2\frac{(1-s)k\cdot p}{s} - \frac{m^2\xi^2 s^2}{2(s-1)}hh' + \frac{m\xi s}{2(s-1)}X_\varepsilon(h+h') - \frac{2}{s^2}X_\varepsilon^2, \tag{A9}$$

$$\mathsf{IP}_1 = i\xi m^2\,\theta\langle\dot{h}\rangle\,\frac{s(2-s)}{2(1-s)}, \tag{A10}$$

$$\mathsf{IP}_2 = -i\xi m^2\,\theta\langle\dot{h}\rangle\,\frac{s^2}{2(1-s)}, \tag{A11}$$

$$\mathsf{FP}_1 = i\xi m^2\,\theta\langle\dot{h}\rangle\,\frac{s(2-s)}{2(1-s)}, \tag{A12}$$

$$\mathsf{FP}_2 = i\xi m^2\,\theta\langle\dot{h}\rangle\,\frac{s^2}{2(1-s)}, \tag{A13}$$

$$\mathsf{PC}_1 = q\cdot p - m^2 - \frac{m^2\xi^2(s-2)^2}{2(s-1)}hh' + \frac{m\xi(s-2)^2}{2(s-1)s}X_\varepsilon(h+h') + \frac{2}{s^2}X_\varepsilon^2 + \frac{X_\beta^2}{s-1}, \tag{A14}$$

$$\mathsf{PC}_2 = -3q\cdot p + m^2 + \frac{2k\cdot q}{s} + \frac{2(1-s)k\cdot p}{s} + \frac{m^2\xi^2 s^2}{2(s-1)}hh' - \frac{m\xi s}{2(s-1)}X_\varepsilon(h+h') - \frac{2}{s^2}X_\varepsilon^2 - \frac{X_\beta^2}{s-1}. \tag{A15}$$

By using the kinematic relations from above some of the expressions can be simplified, e.g., $q\cdot p - m^2 = Ls\kappa\cdot p$. With these replacements it is straightforward to see that all traces depend on the transverse photon momentum only quadratically at most. Here we used that the light-front Levi-Cevita tensor $\epsilon^{+-xy} = -2$, i.e., that Levi-Civita terms occurring in traces with exactly one γ^5 matrix can be simplified as $\epsilon^{p\beta\epsilon\kappa} = p\cdot\kappa$.

2. Gaussian transverse momentum integrals

We find that the transverse momentum integrals over $\boldsymbol{r}_\perp$ are all Gaussian for all eight Compton traces. This fact has been customarily exploited in calculations of spin-averaged nonlinear Compton scattering, to analytically perform the transverse momentum integrals. Here the relevant integrals for polarized NLC read

$$\mathcal{G}_0 = \int d^2\boldsymbol{r}_\perp\, e^{i\theta\frac{k\cdot\langle\pi p\rangle}{\kappa\cdot q}} = \frac{\pi}{-i\theta x_0}\,e^{i\theta x_0\mu}, \tag{A16}$$

$$\mathcal{G}_{1,\varepsilon} = \int d^2\boldsymbol{r}_\perp\, X_\varepsilon\, e^{i\theta\frac{k\cdot\langle\pi p\rangle}{\kappa\cdot q}} = ms\xi\langle h\rangle\mathcal{G}_0, \tag{A17}$$

$$\mathcal{G}_{2,\varepsilon} = \int d^2\boldsymbol{r}_\perp\, X_\varepsilon^2\, e^{i\theta\frac{k\cdot\langle\pi p\rangle}{\kappa\cdot q}} = m^2 s^2\Big[\xi^2\langle h\rangle^2 + \frac{1}{-2i\theta x_0}\Big]\mathcal{G}_0, \tag{A18}$$

$$\mathcal{G}_{1,\beta} = \int d^2\boldsymbol{r}_\perp\, X_\beta\, e^{i\theta\frac{k\cdot\langle\pi p\rangle}{\kappa\cdot q}} = 0, \tag{A19}$$

$$\mathcal{G}_{2,\beta} = \int d^2\boldsymbol{r}_\perp\, X_\beta^2\, e^{i\theta\frac{k\cdot\langle\pi p\rangle}{\kappa\cdot q}} = \frac{m^2 s^2}{-2i\theta x_0}\mathcal{G}_0, \tag{A20}$$

with x_0 defined in Eq. (A7). With these, we find (we omit the leading factor $\mathcal{G}_0$ here which has to be multiplied to all traces)

$$\mathsf{UP}_1 \to (g-1)m^2 + i\frac{gm^2}{\theta x_0} + m^2\xi^2(g+1)(h-\langle h\rangle)(h'-\langle h\rangle), \tag{A21}$$

$$\mathsf{UP}_2 \to (g-1)m^2 + i\frac{gm^2}{\theta x_0} + m^2\xi^2(g-1)(h-\langle h\rangle)(h'-\langle h\rangle), \tag{A22}$$

$$\mathsf{IP}_1 \to i\xi m^2\,\theta\langle\dot h\rangle\,(g-1+s), \tag{A23}$$

$$\mathsf{IP}_2 \to -i\xi m^2\,\theta\langle\dot h\rangle\,(g-1), \tag{A24}$$

$$\mathsf{FP}_1 \to i\xi m^2\,\theta\langle\dot h\rangle\,(g-1+s), \tag{A25}$$

$$\mathsf{FP}_2 \to i\xi m^2\,\theta\langle\dot h\rangle\,(g-1), \tag{A26}$$

$$\mathsf{PC}_1 \to (g-1)m^2 + i\frac{m^2}{\theta x_0} + m^2\xi^2(g+1)(h-\langle h\rangle)(h'-\langle h\rangle), \tag{A27}$$

$$\mathsf{PC}_2 \to -(g-1)m^2 + i\frac{m^2}{\theta x_0} - m^2\xi^2(g-1)(h-\langle h\rangle)(h'-\langle h\rangle). \tag{A28}$$

3. Short coherence interval approximation and θ integrals

With the transverse momentum integrals done, the next step towards the LCFA is to expand the integrand of the θ integral to lowest nontrivial order in the short coherence interval $\theta \ll 1$. This allows us to perform the θ integrals analytically. (Note that one can alternatively perform the θ integral first, and not perform the $\boldsymbol{r}_\perp$ integrals, which leads to an angularly resolved LCFA; see, for instance, Ref. [136].) For the Kibble mass in the exponent that means $\mu \to \mu_0 = 1 + \xi^2\dot h^2\theta^2/12$ [94]. Furthermore, in the preexponential terms we use $\theta\langle\dot h\rangle \to \theta\dot h = \xi^2\dot h^2(\varphi)$ and

$$(h'-\langle h\rangle)(h-\langle h\rangle) \simeq -\frac{\theta^2}{4}\dot h^2. \tag{A29}$$

Inserting the small-θ approximated prefactor $\mathcal{G}_0 \simeq 2\pi b_p\,\frac{1-s}{s}\frac{e^{i\theta x_0\mu_0}}{-i\theta}$ we obtain

$$\int d\boldsymbol{r}_\perp\, e^{i\theta\frac{k\cdot\langle\pi p\rangle}{\kappa\cdot q}}\mathsf{UP}_1 \simeq 2\pi b_p m^2\,\frac{1-s}{s}e^{i\theta x_0\mu_0}\Big[-\frac{g}{\theta^2 x_0} + \frac{i(g-1)}{\theta} - i\theta(g+1)\frac{\dot h^2\xi^2}{4}\Big], \tag{A30}$$

$$\int d\boldsymbol{r}_\perp\, e^{i\theta\frac{k\cdot\langle\pi p\rangle}{\kappa\cdot q}}\mathsf{UP}_2 \simeq 2\pi b_p m^2\,\frac{1-s}{s}e^{i\theta x_0\mu_0}\Big[-\frac{g}{\theta^2 x_0} + \frac{i(g-1)}{\theta} - i\theta(g-1)\frac{\dot h^2\xi^2}{4}\Big], \tag{A31}$$

$$\int d^2\boldsymbol{r}_\perp\, e^{i\theta\frac{k\cdot\langle\pi p\rangle}{\kappa\cdot q}}\mathsf{IP}_1 \simeq -2\pi m^2 b_p\frac{1-s}{s}\,e^{i\theta x_0\mu_0}\,\xi\dot h\,(g-1+s), \tag{A32}$$

$$\int d^2\boldsymbol{r}_\perp\, e^{i\theta\frac{k\cdot\langle\pi p\rangle}{\kappa\cdot q}}\mathsf{IP}_2 \simeq 2\pi m^2 b_p\frac{1-s}{s}\,e^{i\theta x_0\mu_0}\,\xi\dot h\,(g-1), \tag{A33}$$

$$\int d^2\boldsymbol{r}_\perp\, e^{i\theta\frac{k\cdot\langle\pi p\rangle}{\kappa\cdot q}}\mathsf{FP}_1 \simeq -2\pi m^2 b_p\frac{1-s}{s}\,e^{i\theta x_0\mu_0}\,\xi\dot h\,(g-1+s), \tag{A34}$$

$$\int d^2\boldsymbol{r}_\perp\, e^{i\theta\frac{k\cdot\langle\pi p\rangle}{\kappa\cdot q}}\mathsf{FP}_2 \simeq -2\pi m^2 b_p\frac{1-s}{s}\,e^{i\theta x_0\mu_0}\,\xi\dot h\,(g-1), \tag{A35}$$

$$\int d\boldsymbol{r}_\perp\, e^{i\theta\frac{k\cdot\langle\pi p\rangle}{\kappa\cdot q}}\mathsf{PC}_1 \simeq 2\pi b_p m^2\,\frac{1-s}{s}e^{i\theta x_0\mu_0}\Big[-\frac{1}{\theta^2 x_0} + \frac{i(g-1)}{\theta} - i\theta(g+1)\frac{\dot h^2\xi^2}{4}\Big], \tag{A36}$$

$$\int d\boldsymbol{r}_\perp\, e^{i\theta\frac{k\cdot\langle\pi p\rangle}{\kappa\cdot q}}\mathsf{PC}_2 \simeq 2\pi b_p m^2\,\frac{1-s}{s}e^{i\theta x_0\mu_0}\Big[-\frac{1}{\theta^2 x_0} - \frac{i(g-1)}{\theta} + i\theta(g-1)\frac{\dot h^2\xi^2}{4}\Big]. \tag{A37}$$

Next we perform the integrals over the phase variable θ yielding Airy functions

$$\int d\theta\; i\theta\, e^{ix_0\theta + i\frac{\nu}{3}\theta^3} = 2\pi\frac{\mathrm{Ai}\,'(z)}{\sqrt[3]{\nu^2}}, \tag{A38}$$

$$\int d\theta\; e^{ix_0\theta + i\frac{\nu}{3}\theta^3} = 2\pi\frac{\mathrm{Ai}\,(z)}{\sqrt[3]{\nu}}, \tag{A39}$$

$$\int d\theta\; \frac{1}{-i\theta}\, e^{ix_0\theta + i\frac{\nu}{3}\theta^3} = 2\pi\,\mathrm{Ai}_1(z), \tag{A40}$$

$$\int d\theta\; \frac{1}{\theta^2}\, e^{ix_0\theta + i\frac{\nu}{3}\theta^3} = 2\pi x_0\Big[\mathrm{Ai}_1(z) + \frac{\mathrm{Ai}\,'(z)}{z}\Big], \tag{A41}$$

where $\mathrm{Ai}_1(z) = \int_z^\infty dx\,\mathrm{Ai}\,(x)$ and $\mathrm{Ai}\,'(z) = d\mathrm{Ai}\,(z)/dz$.

Here we have rewritten the exponential $e^{i\theta x_0\mu_0} = e^{ix_0\theta + i\frac{y}{3}\theta^3}$ with the definitions

$$y = \frac{x_0\xi^2\dot{h}^2}{4}, \qquad z = \frac{x_0}{\sqrt[3]{y}}. \tag{A42}$$

In addition we use that $\sqrt[3]{y} = \sqrt{z}\xi|\dot{h}|/2$ and thus $\xi\dot{h}/\sqrt[3]{y} = 2\dot{h}/(\sqrt{z}|\dot{h}|) = 2\,\mathrm{sgn}\,(\dot{h})/\sqrt{z}$.

The first and second results follow by the integral definition of the Airy function [137]. The third result can be derived in the following way:

$$\begin{aligned}\int_{-\infty}^{\infty}\frac{d\theta}{\theta}e^{i(r\theta+c_3\theta^3)} &= \lim_{\varepsilon\to 0}\int_{-\infty}^{\infty}\frac{d\theta}{\theta+i\varepsilon}e^{i(r\theta+c_3\theta^3)}\\ &= \lim_{\varepsilon\to 0} -i\int_0^{\infty}dv\int_{-\infty}^{\infty}\frac{d\theta}{\theta+i\varepsilon}e^{i((r+v)\theta+c_3\theta^3)-\varepsilon v\theta}\\ &= -2\pi i\mathrm{Ai}_1\Big[\frac{r}{(3c_3)^{1/3}}\Big],\end{aligned} \tag{A43}$$

and the final result was derived in the Appendix of Ref. [66]. (It turns out the final result is equivalent to integrating once by parts, ignoring the contribution from the pole in the evaluated term, and then using the standard Sokhotsky-Weierstrass method to deal with the pole of the resulting $1/\theta$ integration.)

Here is the collection of all eight NLC traces after the θ integrals have been performed:

$$\int d\theta\int d^2\boldsymbol{r}_\perp\, e^{i\theta\frac{k\cdot\langle\pi_p\rangle}{\kappa\cdot q}}\mathsf{UP}_1 \simeq -4\pi^2m^2b_p\frac{1-s}{s}\Big[\mathrm{Ai}_1(z)+\frac{2g+1}{z}\mathrm{Ai}'(z)\Big], \tag{A44}$$

$$\int d\theta\int d^2\boldsymbol{r}_\perp\, e^{i\theta\frac{k\cdot\langle\pi_p\rangle}{\kappa\cdot q}}\mathsf{UP}_2 \simeq -4\pi^2m^2b_p\frac{1-s}{s}\Big[\mathrm{Ai}_1(z)+\frac{2g-1}{z}\mathrm{Ai}'(z)\Big], \tag{A45}$$

$$\int d\theta\int d^2\boldsymbol{r}_\perp\, e^{i\theta\frac{k\cdot\langle\pi_p\rangle}{\kappa\cdot q}}\mathsf{IP}_1 \simeq -4\pi^2m^2b_p\frac{1-s}{s}\,(g-1+s)\,\frac{2\mathrm{Ai}\,(z)}{\sqrt{z}}\,\mathrm{sgn}\,(\dot{h}), \tag{A46}$$

$$\int d\theta\int d^2\boldsymbol{r}_\perp\, e^{i\theta\frac{k\cdot\langle\pi_p\rangle}{\kappa\cdot q}}\mathsf{IP}_2 \simeq -4\pi^2m^2b_p\frac{1-s}{s}\,(1-g)\,\frac{2\mathrm{Ai}\,(z)}{\sqrt{z}}\,\mathrm{sgn}\,(\dot{h}), \tag{A47}$$

$$\int d\theta\int d^2\boldsymbol{r}_\perp\, e^{i\theta\frac{k\cdot\langle\pi_p\rangle}{\kappa\cdot q}}\mathsf{FP}_1 \simeq -4\pi^2m^2b_p\frac{1-s}{s}\,(g-1+s)\,\frac{2\mathrm{Ai}\,(z)}{\sqrt{z}}\,\mathrm{sgn}\,(\dot{h}), \tag{A48}$$

$$\int d\theta\int d^2\boldsymbol{r}_\perp\, e^{i\theta\frac{k\cdot\langle\pi_p\rangle}{\kappa\cdot q}}\mathsf{FP}_2 \simeq -4\pi^2m^2b_p\frac{1-s}{s}\,(g-1)\,\frac{2\mathrm{Ai}\,(z)}{\sqrt{z}}\,\mathrm{sgn}\,(\dot{h}), \tag{A49}$$

$$\int d\theta\int d^2\boldsymbol{r}_\perp\, e^{i\theta\frac{k\cdot\langle\pi_p\rangle}{\kappa\cdot q}}\mathsf{PC}_1 \simeq -4\pi^2m^2b_p\frac{1-s}{s}\Big[(2-g)\,\mathrm{Ai}_1(z)+\frac{g+2}{z}\,\mathrm{Ai}'(z)\Big], \tag{A50}$$

$$\int d\theta\int d^2\boldsymbol{r}_\perp\, e^{i\theta\frac{k\cdot\langle\pi_p\rangle}{\kappa\cdot q}}\mathsf{PC}_2 \simeq -4\pi^2m^2b_p\frac{1-s}{s}\Big[g\,\mathrm{Ai}_1(z)-\frac{g-2}{z}\,\mathrm{Ai}'(z)\Big]. \tag{A51}$$

By combining these results according to Eq. (33), and by defining the differential probability rate per laser phase as $d\mathbb{R}/ds = d\mathbb{P}/dsd\varphi$ we find

$$\begin{aligned}\frac{d\mathbb{R}_{\mathrm{NLC},1}}{ds}(\sigma_p,\sigma_q) = -\frac{\alpha}{4b_p}\Big\{&[1+\sigma_p\sigma_q(2-g)]\mathrm{Ai}_1(z)+2(\sigma_p+\sigma_q)(g-1+s)\frac{\mathrm{Ai}\,(z)}{\sqrt{z}}\,\mathrm{sgn}\,(\dot{h})\\ &+[2g+1+\sigma_p\sigma_q(g+2)]\frac{\mathrm{Ai}'(z)}{z}\Big\},\end{aligned} \tag{A52}$$

$$\begin{aligned}\frac{d\mathbb{R}_{\mathrm{NLC},2}}{ds}(\sigma_p,\sigma_q) = -\frac{\alpha}{4b_p}\Big\{&(1+\sigma_p\sigma_q g)\mathrm{Ai}_1(z)+2(\sigma_q-\sigma_p)(g-1)\frac{\mathrm{Ai}\,(z)}{\sqrt{z}}\,\mathrm{sgn}\,(\dot{h})\\ &+[2g-1-\sigma_p\sigma_q(g-2)]\frac{\mathrm{Ai}'(z)}{z}\Big\}.\end{aligned} \tag{A53}$$

for a photon to be emitted in polarization state Λ_1 or Λ_2.

APPENDIX B: DETAILS OF THE CALCULATION OF THE LCFA FOR PAIR PRODUCTION

For pair production, the incoming channel is characterized by the scalar product $\kappa\cdot k$, with k the photon four-momentum. The light-front momentum exchange is defined here as $s = p\cdot\kappa/k\cdot\kappa$, where p refers to the *positron* momentum. Hence, for the electron momentum q we have $q\cdot\kappa = (1-s)q\cdot\kappa$. Moreover, we define $\tilde{g} = 1 - \frac{1}{2s(1-s)}$.

By introducing the auxiliary variable $\tilde{L}$, it is possible to express

$$p\cdot q = \tilde{L}k\cdot\kappa - m^2, \tag{B1}$$

$$q\cdot k = \tilde{L}sk\cdot\kappa, \tag{B2}$$

$$p\cdot k = \tilde{L}(1-s)k\cdot\kappa, \tag{B3}$$

where

$$\tilde{L} = \tilde{x}_0\left[1 + s^2\Big(\boldsymbol{r}_\perp - \frac{\boldsymbol{k}_\perp}{m}\Big)^2\right] = \frac{m^2 + Y_\varepsilon^2 + Y_\beta^2}{2s(1-s)k\cdot\kappa} \tag{B4}$$

with

$$\tilde{x}_0 = \frac{1}{2b_k s(1-s)} \tag{B5}$$

and $Y_\varepsilon = p\cdot\varepsilon - sk\cdot\varepsilon$ and $Y_\beta = p\cdot\beta - sk\cdot\beta$, and the normalized transverse positron momentum $\boldsymbol{r}_\perp = \boldsymbol{p}_\perp/ms$. $b_k = k\cdot\kappa/m^2$ is related to the squared center-of-mass energy of the incident photons and can be related to the kinematic pair production threshold of linear Breit-Wheeler via $\tilde{L}b_k \geqslant 2$, or $\tilde{L} \geqslant 2/b_k$.

The dynamic phase of the pair production matrix element reads (without and with the floating average)

$$\frac{-k\cdot\pi_{-p}}{\kappa\cdot q} = \frac{1}{2k\cdot\kappa s(1-s)}\big[m^2 + (Y_\varepsilon - m\xi h)^2 + Y_\beta^2\big], \tag{B6}$$

$$\begin{aligned}\frac{-k\cdot\langle\pi_{-p}\rangle}{\kappa\cdot q} &= \frac{1}{2k\cdot\kappa s(1-s)}\big[m^2\mu + (Y_\varepsilon - m\xi\langle h\rangle)^2 + Y_\beta^2\big] \\ &= \tilde{x}_0[\mu + s^2(\boldsymbol{r}_\perp + \langle\boldsymbol{a}_\perp\rangle/s - \boldsymbol{u}_\perp)^2],\end{aligned} \tag{B7}$$

with the Kibble mass μ, Eq. (26).

1. NBW traces

The NBW, Eqs. (53)–(56), traces are calculated in an analogous way to the NLC traces,

$$\begin{aligned}\mathsf{UP}_1 &= q\cdot p + m^2 - \frac{m^2\xi^2(1-2s)^2}{2(s-1)s}hh' \\ &\quad + \frac{m\xi(1-2s)^2}{2(s-1)s}(h+h')Y_\varepsilon - 2Y_\varepsilon^2,\end{aligned} \tag{B8}$$

$$\begin{aligned}\mathsf{UP}_2 &= -q\cdot p + m^2 + 2(1-s)k\cdot p + 2sk\cdot q - \frac{m^2\xi^2}{2(s-1)s}hh' \\ &\quad + \frac{m\xi}{2(s-1)s}(h+h')Y_\varepsilon + 2Y_\varepsilon^2,\end{aligned} \tag{B9}$$

$$\mathsf{PP}_1 = im^2\xi\,\theta\langle\dot{h}\rangle\,\frac{2s-1}{2s(1-s)}, \tag{B10}$$

$$\mathsf{PP}_2 = -im^2\xi\,\theta\langle\dot{h}\rangle\,\frac{1}{2s(1-s)}, \tag{B11}$$

$$\mathsf{EP}_1 = im^2\xi\,\theta\langle\dot{h}\rangle\,\frac{2s-1}{2s(1-s)}, \tag{B12}$$

$$\mathsf{EP}_2 = im^2\xi\,\theta\langle\dot{h}\rangle\,\frac{1}{2s(1-s)}, \tag{B13}$$

$$\begin{aligned}\mathsf{PC}_1 &= q\cdot p + m^2 - \frac{m^2\xi^2(1-2s)^2}{2(s-1)s}hh' \\ &\quad + \frac{m\xi(1-2s)^2}{2(s-1)s}(h+h')Y_\varepsilon - 2Y_\varepsilon^2 + \frac{Y_\beta^2}{(s-1)s},\end{aligned} \tag{B14}$$

$$\begin{aligned}\mathsf{PC}_2 &= -3q\cdot p - m^2 + 2(1-s)k\cdot p + 2sk\cdot q + \frac{m^2\xi^2}{2(s-1)s}hh' \\ &\quad - \frac{m\xi}{2(s-1)s}(h+h')Y_\varepsilon + 2Y_\varepsilon^2 - \frac{Y_\beta^2}{(s-1)s}.\end{aligned} \tag{B15}$$

By employing the kinematic relations from above it is straightforward to see that all transverse momentum integrals over the eight traces are Gaussian.

2. Gaussian transverse momentum integrals for NBW

For NBW pair production, all transverse momentum integrals over $d^2\boldsymbol{r}_\perp$ are Gaussian as well. However, the expression of the dynamic phase is slightly different, and so are the results:

$$\tilde{\mathfrak{G}}_0 = \int d^2\boldsymbol{r}_\perp\, e^{i\theta\frac{-k\cdot\langle\pi_{-p}\rangle}{\kappa\cdot q}} = e^{i\theta\tilde{x}_0\mu}\frac{\pi}{-i\theta\tilde{x}_0 s^2}, \tag{B16}$$

$$\tilde{\mathfrak{G}}_{1,\varepsilon} = \int d^2\boldsymbol{r}_\perp\, Y_\varepsilon\, e^{i\theta\frac{-k\cdot\langle\pi_{-p}\rangle}{\kappa\cdot q}} = m\xi\langle h\rangle\tilde{\mathfrak{G}}_0, \tag{B17}$$

$$\tilde{\mathfrak{G}}_{2,\varepsilon} = \int d^2\boldsymbol{r}_\perp\, Y_\varepsilon^2\, e^{i\theta\frac{-k\cdot\langle\pi_{-p}\rangle}{\kappa\cdot q}} = \left[m^2\xi^2\langle h\rangle^2 + \frac{m^2}{-2i\tilde{\theta}x_0}\right]\tilde{\mathfrak{G}}_0, \tag{B18}$$

$$\tilde{\mathfrak{G}}_{1,\beta} = \int d^2\boldsymbol{r}_\perp\, Y_\beta\, e^{i\theta\frac{k\cdot\langle\pi\rangle}{\kappa\cdot q}} = 0, \tag{B19}$$

$$\tilde{\mathfrak{G}}_{2,\beta} = \int d^2\boldsymbol{r}_\perp\, Y_\beta^2\, e^{i\theta\frac{k\cdot\langle\pi\rangle}{\kappa\cdot q}} = \frac{m^2}{-2i\theta\tilde{x}_0}\tilde{\mathfrak{G}}_0, \tag{B20}$$

with $\tilde{x}_0$ defined in Eq. (B5). Employing those Gaussian integrals, the eight NBW traces turn to the following expressions, omitting again the leading factor $\tilde{\mathfrak{G}}_0$:

$$\begin{aligned}\mathsf{UP}_1 \to{}& (1-\tilde{g})m^2 - \frac{i\tilde{g}m^2}{\theta\tilde{x}_0} \\ &-(1+\tilde{g})m^2\xi^2(h-\langle h\rangle)(h'-\langle h\rangle),\end{aligned} \tag{B21}$$

$$\begin{aligned}\mathsf{UP}_2 \to{}& (1-\tilde{g})m^2 - \frac{i\tilde{g}m^2}{\theta\tilde{x}_0} \\ &+(1-\tilde{g})m^2\xi^2(h-\langle h\rangle)(h'-\langle h\rangle),\end{aligned} \tag{B22}$$

$$\mathsf{PP}_1 \to -im^2\xi\,\theta\langle\dot{h}\rangle\,(\tilde{g}-1+s^{-1}), \tag{B23}$$

$$\mathsf{PP}_2 \to im^2\xi\,\theta\langle\dot{h}\rangle\,(\tilde{g}-1), \tag{B24}$$

$$\mathsf{EP}_1 \to -im^2\xi\,\theta\langle\dot{h}\rangle\,(\tilde{g}-1+s^{-1}), \tag{B25}$$

$$\mathsf{EP}_2 \to -im^2\xi\,\theta\langle\dot{h}\rangle\,(\tilde{g}-1), \tag{B26}$$

$$\begin{aligned}\mathsf{PC}_1 \to{}& (1-\tilde{g})m^2 - \frac{im^2}{\theta\tilde{x}_0} \\ &-(1+\tilde{g})m^2\xi^2(h-\langle h\rangle)(h'-\langle h\rangle),\end{aligned} \tag{B27}$$

$$\begin{aligned}\mathsf{PC}_2 \to{}& -(1-\tilde{g})m^2 - \frac{im^2}{\theta\tilde{x}_0}. \\ &-(1-\tilde{g})m^2\xi^2(h-\langle h\rangle)(h'-\langle h\rangle)\end{aligned} \tag{B28}$$

3. Short coherence interval approximation and θ integrals

The next step towards the LCFA for NBW is approximating the integrand for short coherence interval $\theta \ll 1$. This is exactly the same as for NLC. The only notable difference is that we have to insert here the small-θ approximation

of $\tilde{\mathcal{G}}_0 \simeq e^{i\theta\tilde{x}_0\mu_0}\frac{\pi}{-i\theta\tilde{x}_0 s^2} = 2\pi b_k \frac{1-s}{s}\frac{e^{i\theta\tilde{x}_0\mu_0}}{-i\theta}$:

$$\int d^2\boldsymbol{r}_\perp\, e^{i\theta\frac{-k\cdot\langle\pi-p\rangle}{\kappa\cdot q}}\,\mathsf{UP}_1 \simeq 2\pi b_k m^2 \frac{1-s}{s}\, e^{i\theta\tilde{x}_0\mu_0}\left[i\theta\frac{\xi^2\dot{h}^2}{4}(\tilde{g}+1)+\frac{i(1-\tilde{g})}{\theta}+\frac{\tilde{g}}{\theta^2\tilde{x}_0}\right], \tag{B29}$$

$$\int d^2\boldsymbol{r}_\perp\, e^{i\theta\frac{-k\cdot\langle\pi-p\rangle}{\kappa\cdot q}}\,\mathsf{UP}_2 \simeq 2\pi b_k m^2 \frac{1-s}{s}\, e^{i\theta\tilde{x}_0\mu_0}\left[i\theta\frac{\xi^2\dot{h}^2}{4}(\tilde{g}-1)+\frac{i(1-\tilde{g})}{\theta}+\frac{\tilde{g}}{\theta^2\tilde{x}_0}\right], \tag{B30}$$

$$\int d^2\boldsymbol{r}_\perp\, e^{i\theta\frac{-k\cdot\langle\pi-p\rangle}{\kappa\cdot q}}\,\mathsf{PP}_1 \simeq 2\pi m^2 b_k \frac{1-s}{s}\, e^{i\theta\tilde{x}_0\mu_0}\,\xi\dot{h}\left(\tilde{g}-1+\frac{1}{s}\right), \tag{B31}$$

$$\int d^2\boldsymbol{r}_\perp\, e^{i\theta\frac{-k\cdot\langle\pi-p\rangle}{\kappa\cdot q}}\,\mathsf{PP}_2 \simeq 2\pi m^2 b_k \frac{1-s}{s}\, e^{i\theta\tilde{x}_0\mu_0}\,\xi\dot{h}\,(1-\tilde{g}), \tag{B32}$$

$$\int d^2\boldsymbol{r}_\perp\, e^{i\theta\frac{-k\cdot\langle\pi-p\rangle}{\kappa\cdot q}}\,\mathsf{EP}_1 \simeq 2\pi m^2 b_k \frac{1-s}{s}\, e^{i\theta\tilde{x}_0\mu_0}\,\xi\dot{h}\left(\tilde{g}-1+\frac{1}{s}\right), \tag{B33}$$

$$\int d^2\boldsymbol{r}_\perp\, e^{i\theta\frac{-k\cdot\langle\pi-p\rangle}{\kappa\cdot q}}\,\mathsf{EP}_2 \simeq 2\pi m^2 b_k \frac{1-s}{s}\, e^{i\theta\tilde{x}_0\mu_0}\,\xi\dot{h}\,(\tilde{g}-1), \tag{B34}$$

$$\int d^2\boldsymbol{r}_\perp\, e^{i\theta\frac{-k\cdot\langle\pi-p\rangle}{\kappa\cdot q}}\,\mathsf{PC}_1 \simeq 2\pi b_k m^2 \frac{1-s}{s}\, e^{i\theta\tilde{x}_0\mu_0}\left[i\theta\frac{\xi^2\dot{h}^2}{4}(1+\tilde{g})+\frac{i(1-\tilde{g})}{\theta}+\frac{1}{\theta^2\tilde{x}_0}\right], \tag{B35}$$

$$\int d^2\boldsymbol{r}_\perp\, e^{i\theta\frac{-k\cdot\langle\pi-p\rangle}{\kappa\cdot q}}\,\mathsf{PC}_2 \simeq 2\pi b_k m^2 \frac{1-s}{s}\, e^{i\theta\tilde{x}_0\mu_0}\left[i\theta\frac{\xi^2\dot{h}^2}{4}(1-\tilde{g})-\frac{i(1-\tilde{g})}{\theta}+\frac{1}{\theta^2\tilde{x}_0}\right]. \tag{B36}$$

Next we have to perform the integrals over θ which will yield the Airy functions.

The results of the θ integration are formally the same as for Compton, Eqs. (A38)–(A41), but with the replacements $x_0 \to \tilde{x}_0$, $y \to \tilde{y}$ and $z \to \tilde{z}$, where

$$\tilde{y} = \frac{\tilde{x}_0\xi^2\dot{h}^2}{4}, \qquad \tilde{z} = \frac{\tilde{x}_0}{\sqrt[3]{\tilde{y}}} = \left[\frac{1}{\chi_k|\dot{h}|s(1-s)}\right]^{2/3}. \tag{B37}$$

With these results we obtain for the eight NBW pair production traces:

$$\int d\theta\int d^2\boldsymbol{r}_\perp\, e^{i\theta\frac{-k\cdot\langle\pi-p\rangle}{\kappa\cdot q}}\,\mathsf{UP}_1 \simeq 4\pi^2 m^2 b_k \frac{1-s}{s}\left[\mathrm{Ai}_1(\tilde{z})+\frac{2\tilde{g}+1}{\tilde{z}}\,\mathrm{Ai}'(\tilde{z})\right], \tag{B38}$$

$$\int d\theta\int d^2\boldsymbol{r}_\perp\, e^{i\theta\frac{-k\cdot\langle\pi-p\rangle}{\kappa\cdot q}}\,\mathsf{UP}_2 \simeq 4\pi^2 m^2 b_k \frac{1-s}{s}\left[\mathrm{Ai}_1(\tilde{z})+\frac{2\tilde{g}-1}{\tilde{z}}\,\mathrm{Ai}'(\tilde{z})\right], \tag{B39}$$

$$\int d\theta\int d^2\boldsymbol{r}_\perp\, e^{i\theta\frac{-k\cdot\langle\pi-p\rangle}{\kappa\cdot q}}\,\mathsf{PP}_1 \simeq 4\pi^2 m^2 b_k \frac{1-s}{s}\,\frac{\mathrm{Ai}(\tilde{z})}{\sqrt{\tilde{z}}}\,2\left(\tilde{g}-1+\frac{1}{s}\right)\mathrm{sgn}(\dot{h}), \tag{B40}$$

$$\int d\theta\int d^2\boldsymbol{r}_\perp\, e^{i\theta\frac{-k\cdot\langle\pi-p\rangle}{\kappa\cdot q}}\,\mathsf{PP}_2 \simeq 4\pi^2 m^2 b_k \frac{1-s}{s}\,\frac{\mathrm{Ai}(\tilde{z})}{\sqrt{\tilde{z}}}\,2(1-\tilde{g})\,\mathrm{sgn}(\dot{h}), \tag{B41}$$

$$\int d\theta\int d^2\boldsymbol{r}_\perp\, e^{i\theta\frac{-k\cdot\langle\pi-p\rangle}{\kappa\cdot q}}\,\mathsf{EP}_1 \simeq 4\pi^2 m^2 b_k \frac{1-s}{s}\,\frac{\mathrm{Ai}(\tilde{z})}{\sqrt{\tilde{z}}}\,2\left(\tilde{g}-1+\frac{1}{s}\right)\mathrm{sgn}(\dot{h}), \tag{B42}$$

$$\int d\theta\int d^2\boldsymbol{r}_\perp\, e^{i\theta\frac{-k\cdot\langle\pi-p\rangle}{\kappa\cdot q}}\,\mathsf{EP}_2 \simeq 4\pi^2 m^2 b_k \frac{1-s}{s}\,\frac{\mathrm{Ai}(\tilde{z})}{\sqrt{\tilde{z}}}\,2(\tilde{g}-1)\,\mathrm{sgn}(\dot{h}), \tag{B43}$$

$$\int d\theta\int d^2\boldsymbol{r}_\perp\, e^{i\theta\frac{-k\cdot\langle\pi-p\rangle}{\kappa\cdot q}}\,\mathsf{PC}_1 \simeq 4\pi^2 m^2 b_k \frac{1-s}{s}\left[(2-\tilde{g})\,\mathrm{Ai}_1(\tilde{z})+\frac{2+\tilde{g}}{\tilde{z}}\,\mathrm{Ai}'(\tilde{z})\right], \tag{B44}$$

$$\int d\theta\int d^2\boldsymbol{r}_\perp\, e^{i\theta\frac{-k\cdot\langle\pi-p\rangle}{\kappa\cdot q}}\,\mathsf{PC}_2 \simeq 4\pi^2 m^2 b_k \frac{1-s}{s}\left[\tilde{g}\mathrm{Ai}_1(\tilde{z})+\frac{2-\tilde{g}}{\tilde{z}}\,\mathrm{Ai}'(\tilde{z})\right]. \tag{B45}$$

Combining these traces by plugging them into

$$\frac{d\mathbb{R}_{\mathrm{NBW},j}}{ds}(\sigma_p,\sigma_q) = \frac{\alpha}{16\pi^2 m^2 b_k^2}\frac{s}{1-s}\int d\theta\int d^2\boldsymbol{r}_\perp\, e^{i\theta\frac{-k\cdot\langle\pi-p\rangle}{\kappa\cdot q}}[\mathsf{UP}_j+\sigma_q\mathsf{EP}_j+\sigma_p\mathsf{PP}_j+\sigma_p\sigma_q\mathsf{PC}_j], \tag{B46}$$

we get the LCFA expressions for the decay rate per unit laser phase of a polarized photon in a polarization state Λ_j, $j=1,2$, into a polarized electron-positron pair:

$$\frac{d\mathbb{R}_{\mathrm{NBW},1}}{ds}(\sigma_p,\sigma_q) = \frac{\alpha}{4b_k}\left\{[(1+\sigma_p\sigma_q(2-\tilde{g})]\mathrm{Ai}_1(\tilde{z})-2(\sigma_p+\sigma_q)\left(1-\tilde{g}-\frac{1}{s}\right)\frac{\mathrm{Ai}(\tilde{z})}{\sqrt{\tilde{z}}}\,\mathrm{sgn}(\dot{h})\right.$$

$$+ [2\tilde{g} + 1 + \sigma_p\sigma_q(2 + \tilde{g})]\frac{\mathrm{Ai}'(\tilde{z})}{\tilde{z}}\Bigg\}, \tag{B47}$$

$$\frac{d\mathbb{R}_{\mathrm{NBW},2}}{ds}(\sigma_p, \sigma_q) = \frac{\alpha}{4b_k}\Bigg\{[(1 + \sigma_p\sigma_q\tilde{g}]\mathrm{Ai}_1(\tilde{z}) + 2(\sigma_p - \sigma_q)(1 - \tilde{g})\frac{\mathrm{Ai}(\tilde{z})}{\sqrt{\tilde{z}}}\,\mathrm{sgn}(\dot{h})$$

$$+ [2\tilde{g} - 1 + \sigma_p\sigma_q(2 - \tilde{g})]\frac{\mathrm{Ai}'(\tilde{z})}{\tilde{z}}\Bigg\}. \tag{B48}$$

By introducing again the Stokes parameter for the incoming photon we arrive at Eq. (59).

[1] J. M. Cole, K. T. Behm, E. Gerstmayr, T. G. Blackburn, J. C. Wood, C. D. Baird, M. J. Duff, C. Harvey, A. Ilderton, A. S. Joglekar *et al.*, Experimental Evidence of Radiation Reaction in the Collision of a High-Intensity Laser Pulse with a Laser-Wakefield Accelerated Electron Beam, Phys. Rev. X **8**, 011020 (2018).

[2] K. Poder, M. Tamburini, G. Sarri, A. Di Piazza, S. Kuschel, C. D. Baird, K. Behm, S. Bohlen, J. M. Cole, D. J. Corvan *et al.*, Experimental Signatures of the Quantum Nature of Radiation Reaction in the Field of an Ultraintense Laser, Phys. Rev. X **8**, 031004 (2018).

[3] M. Aléonard, M. Altarelli, P. Antici, A. Apolonskiy, P. Audebert, A. Bartnik, C. Barty, A. Bernstein, J. Biegert, P. Böni *et al.*, *WHITEBOOK ELI—Extreme Light Infrastructure; Science and Technology with Ultra-Intense Lasers*, edited by G. A. Mourou, G. Korn, W. Sandner, and J. L. Collier (THOSS Media GmbH, Berlin, Germany, 2011).

[4] K. A. Tanaka, K. M. Spohr, D. L. Balabanski, S. Balascuta, L. Capponi, M. O. Cernaianu, M. Cuciuc, A. Cucoanes, I. Dancus, A. Dhal *et al.*, Current status and highlights of the ELI-NP research program, Matter Radiat. Extrem. **5**, 024402 (2020).

[5] J. W. Yoon, C. Jeon, J. Shin, S. K. Lee, H. W. Lee, I. W. Choi, H. T. Kim, J. H. Sung, and C. H. Nam, Achieving the laser intensity of 5.5×10^{22} W/cm^2 with a wavefront-corrected multi-PW laser, Opt. Express **27**, 20412 (2019).

[6] J. Bromage, S.-W. Bahk, I. Begishev, C. Dorrer, M. Guardalben, B. Hoffman, J. Oliver, R. Roides, E. Schiesser, M. Shoup *et al.*, Technology development for ultraintense all-OPCPA systems, High Power Laser Sci. Eng. **7**, e4 (2019).

[7] B. Shen, B. Zhigang, J. Xu, T. Xu, L. Ji, R. Li, and Z. Xu, Exploring vacuum birefringence based on a 100 PW laser and an X-ray free electron laser beam, Plasma Phys. Controlled Fusion **60**, 044002 (2018).

[8] C. N. Danson, C. Haefner, J. Bromage, T. Butcher, J.-C. F. Chanteloup, E. A. Chowdhury, A. Galvanauskas, L. A. Gizzi, J. Hein, D. I. Hillier *et al.*, Petawatt and exawatt class lasers worldwide, High Power Laser Sci. Eng. **7**, e54 (2019).

[9] A. I. Nikishov and V. I. Ritus, Quantum processes in the field of a plane electromagnetic wave and in a constant field I, Sov. Phys. JETP **19**, 529 (1964).

[10] L. S. Brown and T. W. B. Kibble, Interaction of intense laser beams with electrons, Phys. Rev. **133**, A705 (1964).

[11] N. B. Narozhny, A. I. Nikishov, and V. I. Ritus, Quantum processes in the field of a circularly polarized electromagnetic wave, Sov. Phys. JETP **20**, 622 (1965).

[12] H. R. Reiss, Absorption of light by light, J. Math. Phys. **3**, 59 (1962).

[13] K. Horikawa, S. Miyamoto, T. Mochizuki, S. Amano, D. Li, K. Imasaki, Y. Izawa, K. Ogata, S. Chiba, and T. Hayakawa, Neutron angular distribution in (γ, n) reactions with linearly polarized γ-ray beam generated by laser Compton scattering, Phys. Lett. B **737**, 109 (2014).

[14] A. Ilderton and M. Marklund, Prospects for studying vacuum polarization using dipole and synchrotron radiation, J. Plasma Phys. **82**, 655820201 (2016).

[15] B. King and N. Elkina, Vacuum birefringence in high-energy laser-electron collisions, Phys. Rev. A **94**, 062102 (2016).

[16] Y. Nakamiya and K. Homma, Probing vacuum birefringence under a high-intensity laser field with gamma-ray polarimetry at the GeV scale, Phys. Rev. D **96**, 053002 (2017).

[17] S. Bragin, S. Meuren, C. H. Keitel, and A. Di Piazza, High-Energy Vacuum Birefringence and Dichroism in an Ultrastrong Laser Field, Phys. Rev. Lett. **119**, 250403 (2017).

[18] V. I. Ritus, Vacuum polarisation correction to elastic electron and muon scattering in an intense field and pair electro- and muoproduction, Nucl. Phys. B **44**, 236 (1972).

[19] D. A. Morozov and N. B. Narozhnyi, Elastic scattering of photons in an intense field and pair and photon photoproduction of a pair and a photon, Sov. Phys. JETP **45**, 23 (1977).

[20] H. Hu, C. Müller, and C. H. Keitel, Complete QED Theory of Multiphoton Trident Pair Production in Strong Laser Fields, Phys. Rev. Lett. **105**, 080401 (2010).

[21] A. Ilderton, Trident Pair Production in Strong Laser Pulses, Phys. Rev. Lett. **106**, 020404 (2011).

[22] B. King and H. Ruhl, The trident process in a constant crossed field, Phys. Rev. D **88**, 013005 (2013).

[23] V. Dinu and G. Torgrimsson, Trident pair production in plane waves: Coherence, exchange, and spacetime inhomogeneity, Phys. Rev. D **97**, 036021 (2018).

[24] F. Mackenroth and A. Di Piazza, Nonlinear trident pair production in an arbitrary plane wave: A focus on the properties of the transition amplitude, Phys. Rev. D **98**, 116002 (2018).

[25] B. King and A. M. Fedotov, Effect of interference on the trident process in a constant crossed field, Phys. Rev. D **98**, 016005 (2018).

[26] V. Dinu and G. Torgrimsson, Trident process in laser pulses, Phys. Rev. D **101**, 056017 (2020).

[27] G. Torgrimsson, Nonlinear trident in the high-energy limit: Nonlocality, Coulomb field and resummations, arXiv:2007.08492 [hep-ph] (2020).

[28] D. A. Morozov and V. I. Ritus, Elastic electron scattering in an intense field and two-photon emission, Nucl. Phys. B **86**, 309 (1975).

[29] D. Seipt and B. Kämpfer, Two-photon Compton process in pulsed intense laser fields, Phys. Rev. D **85**, 101701(R) (2012).

[30] F. Mackenroth and A. Di Piazza, Nonlinear Double Compton Scattering in the Ultrarelativistic Quantum Regime, Phys. Rev. Lett. **110**, 070402 (2013).

[31] B. King, Double Compton scattering in a constant crossed field, Phys. Rev. A **91**, 033415 (2015).

[32] V. Dinu and G. Torgrimsson, Single and double nonlinear Compton scattering, Phys. Rev. D **99**, 096018 (2019).

[33] E. N. Nerush, I. Yu. Kostyukov, A. M. Fedotov, N. B. Narozhny, N. V. Elkina, and H. Ruhl, Laser Field Absorption in Self-Generated Electron-Positron Pair Plasma, Phys. Rev. Lett. **106**, 035001 (2011).

[34] A. A. Mironov, N. B. Narozhny, and A. M. Fedotov, Collapse and revival of electromagnetic cascades in focused intense laser pulses, Phys. Lett. A **378**, 3254 (2014).

[35] V. F. Bashmakov, E. N. Nerush, I. Yu. Kostyukov, A. M. Fedotov, and N. B. Narozhny, Effect of laser polarization on quantum electrodynamical cascading, Phys. Plasmas **21**, 013105 (2014).

[36] E. G. Gelfer, A. A. Mironov, A. M. Fedotov, V. F. Bashmakov, E. N. Nerush, I. Yu. Kostyukov, and N. B. Narozhny, Optimized multibeam configuration for observation of QED cascades, Phys. Rev. A **92**, 022113 (2015).

[37] N. B. Narozhnyi and A. M. Fedotov, Quantum-electrodynamic cascades in intense laser fields, Phys. Usp. **58**, 95 (2015).

[38] M. Tamburini, A. Di Piazza, and C. H. Keitel, Laser-pulse-shape control of seeded QED cascades, Sci. Rep. **7**, 5694 (2017).

[39] T. Grismayer, M. Vranic, J. L. Martins, R. A. Fonseca, and L. O. Silva, Seeded QED cascades in counterpropagating laser pulses, Phys. Rev. E **95**, 023210 (2017).

[40] P. Zhang, S. S. Bulanov, D. Seipt, A. V. Arefiev, and A. G. R. Thomas, Relativistic plasma physics in supercritical fields, Phys. Plasmas **27**, 050601 (2020).

[41] D. Seipt, C. P. Ridgers, D. Del Sorbo, and A. G. R. Thomas, Polarized QED cascades, arXiv:2010.04078 [hep-ph].

[42] A. V. Borisov and V. Yu. Grishina, Compton production of axions on electrons in a constant external field, Sov. Phys. JETP **83**, 868 (1996).

[43] B. King, Electron-seeded ALP production and ALP decay in an oscillating electromagnetic field, Phys. Lett. B **782**, 737 (2018).

[44] B. M. Dillon and B. King, ALP production through non-linear Compton scattering in intense fields, Eur. Phys. J. C **78**, 775 (2018).

[45] B. King, B. M. Dillon, K. A. Beyer, and G. Gregori, Axion-like-particle decay in strong electromagnetic backgrounds, J. High Energy Phys. 12 (2019) 162.

[46] O. Klein and Y. Nishina, Über die Streuung von Strahlung durch freie Elektronen nach der neuen relativistischen Quantendynamik von Dirac, Z. Phys. **52**, 853 (1929).

[47] U. Fano, Remarks on the classical and quantum-mechanical treatment of partial polarization, J. Opt. Soc. Am. **39**, 859 (1949).

[48] F. W. Lipps and H. A. Tolhoek, Polarization phenomena of electrons and photons. II, Physica **20**, 395 (1954).

[49] G. Bhatt, H. Grotch, E. Kazes, and D. A. Owen, Relativistic spin-dependent Compton scattering from electrons, Phys. Rev. A **28**, 2195 (1983).

[50] S. Ahrens and C.-P. Sun, Spin in Compton scattering with pronounced polarization dynamics, Phys. Rev. A **96**, 063407 (2017).

[51] G. Breit and J. A. Wheeler, Collision of two light quanta, Phys. Rev. **46**, 1087 (1934).

[52] F. Ehlotzky, K. Krajewska, and J. Z. Kamiński, Fundamental processes of quantum electrodynamics in laser fields of relativistic power, Reports Prog. Phys. **72**, 046401 (2009).

[53] M. Boca, V. Dinu, and V. Florescu, Spin effects in nonlinear Compton scattering in a plane-wave laser pulse, Nucl. Instruments Methods Phys. Res. B **279**, 12 (2012).

[54] S. Villalba-Chávez and C. Müller, Photo-production of scalar particles in the field of a circularly polarized laser beam, Phys. Lett. B **718**, 992 (2013).

[55] M. J. A. Jansen, J. Z. Kamiński, K. Krajewska, and C. Müller, Strong-field Breit-Wheeler pair production in short laser pulses: Relevance of spin effects, Phys. Rev. D **94**, 013010 (2016).

[56] K. Kirsebom, U. Mikkelsen, E. Uggerhøj, K. Elsener, S. Ballestrero, P. Sona, and Z. Z. Vilakazi, First Measurements of the Unique Influence of Spin on the Energy Loss of Ultrarelativistic Electrons in Strong Electromagnetic Fields, Phys. Rev. Lett. **87**, 054801 (2001).

[57] K. Krajewska and J. Z. Kamiński, Spin effects in nonlinear Compton scattering in ultrashort linearly-polarized laser pulses, Laser Part. Beams **31**, 503 (2013).

[58] K. Krajewska and J. Z. Kamiński, Frequency scaling law for nonlinear Compton and Thomson scattering: Relevance of spin and polarization effects, Phys. Rev. A **90**, 052117 (2014).

[59] V. N. Baĭer, V. M. Katkov, A. I. Mil'shteĭn, and V. M. Strakhovenko, The theory of quantum processes in the field of a strong electromagnetic wave, Sov. Phys. JETP **42**, 400 (1976).

[60] S. Meuren and A. Di Piazza, Quantum Electron Self-Interaction in a Strong Laser Field, Phys. Rev. Lett. **107**, 260401 (2011).

[61] V. N. Baĭer, Radiative polarization of electrons in storage rings, Sov. Phys. Usp. **14**, 695 (1972).

[62] V. I. Ritus, Quantum effects of the interaction of elementary particles with an intense electromagnetic field, J. Russ. Laser Res. **6**, 497 (1985).

[63] B. King, N. Elkina, and H. Ruhl, Photon polarization in electron-seeded pair-creation cascades, Phys. Rev. A **87**, 042117 (2013).

[64] Y. S. Tsai, Laser $+ e^- \to \gamma + e^-$ and laser $+ \gamma \to e^+ + e^-$ as sources of producing circularly polarized γ and $e^\pm$ beams, Phys. Rev. D **48**, 96 (1993).

[65] S. Tang, B. King, and H. Hu, Highly polarised gamma photons from electron-laser collisions, Phys. Lett. B **809**, 135701 (2020).

[66] B. King and S. Tang, Nonlinear Compton scattering of polarised photons in plane-wave backgrounds, Phys. Rev. A **102**, 022809 (2020).

[67] V. I. Ritus, Radiative effects and their enhancement in an intense electromagnetic field, Sov. Phys. JETP **30**, 1181 (1970).

[68] V. I. Ritus, Radiative corrections in quantum electrodynamics with intense field and their analytical properties, Ann. Phys. **69**, 555 (1972).

[69] E. Bol'shedvorsky, S. Polityko, and A. Misaki, Spin of scattered electrons in the nonlinear Compton effect, Prog. Theor. Phys. **104**, 769 (2000).

[70] D. Yu. Ivanov, G. L. Kotkin, and V. G. Serbo, Complete description of polarization effects in emission of a photon by an electron in the field of a strong laser wave, Eur. Phys. J. C **36**, 127 (2004).

[71] T. N. Wistisen and A. Di Piazza, Numerical approach to the semiclassical method of radiation emission for arbitrary electron spin and photon polarization, Phys. Rev. D **100**, 116001 (2019).

[72] D. Seipt, D. Del Sorbo, C. P. Ridgers, and A. G. R. Thomas, Theory of radiative electron polarization in strong laser fields, Phys. Rev. A **98**, 023417 (2018).

[73] W.-Y. Tsai and A. Yildiz, Motion of an electron in a homogeneous magnetic field-modified propagation function and synchrotron radiation, Phys. Rev. D **8**, 3446 (1973).

[74] J. D. Jackson, On understanding spin-flip synchrotron radiation and the transverse polarization of electrons in storage rings, Rev. Mod. Phys. **48**, 417 (1976).

[75] A. A. Sokolov and I. M. Ternov, *Synchrotron Radiation* (Akademie Verlag, Berlin, 1968).

[76] I. M. Ternov, Synchrotron radiation, Phys. Usp. **38**, 409 (1995).

[77] V. A. Bordovitsyn, I. M. Ternov, and Vladislav G. Bagrov, Spin light, Phys. Usp. **38**, 1037 (1995).

[78] S. R. Mane, Yu. M. Shatunov, and K. Yokoya, Spin-polarized charged particle beams in high-energy accelerators, Reports Prog. Phys. **68**, 1997 (2005).

[79] J. S. Toll, The dispersion relation for light and its application to problems involving electron pairs, Ph.D. thesis, Princeton University, 1952.

[80] A. I. Nikishov and V. I. Ritus, Pair production by a photon and photon emission by an electron in the field of an intense electromagnetic wave and in a constant field, Sov. Phys. JETP **25**, 1135 (1967).

[81] W.-Y Tsai and T. Erber, Photon pair creation in intense magnetic fields, Phys. Rev. D **10**, 492 (1974).

[82] V. Katkov, Production of a pair by a polarized photon in a uniform constant electromagnetic field, J. Exp. Theor. Phys. **114**, 226 (2012).

[83] D. Yu. Ivanov, G. L. Kotkin, and V. G. Serbo, Complete description of polarization effects in e^+e^- pair production by a photon in the field of a strong laser wave, Eur. Phys. J. C **40**, 27 (2005).

[84] T. N. Wistisen, Numerical approach to the semiclassical method of pair production for arbitrary spins and photon polarization, Phys. Rev. D **101**, 076017 (2020).

[85] A. Di Piazza, A. I. Milstein, and C. Müller, Polarization of the electron and positron produced in combined Coulomb and strong laser fields, Phys. Rev. A **82**, 062110 (2010).

[86] T.-O. Müller and C. Müller, Spin correlations in nonperturbative electron-positron pair creation by petawatt laser pulses colliding with a TeV proton beam, Phys. Lett. B **696**, 201 (2011).

[87] C. Kohlfürst, Spin states in multiphoton pair production for circularly polarized light, Phys. Rev. D **99**, 096017 (2019).

[88] X.-G. Huang and H. Taya, Spin-dependent dynamically assisted Schwinger mechanism, Phys. Rev. D **100**, 016013 (2019).

[89] C. F. V. Weizsäcker, Ausstrahlung bei Stößen sehr schneller Elektronen, Z. Phys. **88**, 612 (1934).

[90] E. J. Williams, Nature of the high energy particles of penetrating radiation and status of ionization and radiation formulae, Phys. Rev. **45**, 729 (1934).

[91] H. Abramowicz, M. Altarelli, R. Aßmann, T. Behnke, Y. Benhammou, O. Borysov, M. Borysova, R. Brinkmann, F. Burkart, K. Büßer *et al.*, Letter of intent for the LUXE experiment, arXiv:1909.00860 (2019).

[92] S. Meuren, P. H. Bucksbaum, N. J. Fisch, F. Fiúza, S. Glenzer, M. J. Hogan, K. Qu, D. A. Reis, G. White, and V. Yakimenko, On seminal HEDP research opportunities enabled by colocating multi-petawatt laser with high-density electron beams, arXiv:2002.10051 [physics.plasm-ph] (2020).

[93] T. G. Blackburn, D. Seipt, S. S. Bulanov, and M. Marklund, Benchmarking semiclassical approaches to strong-field QED: Nonlinear Compton scattering in intense laser pulses, Phys. Plasmas **25** (2018).

[94] A. Ilderton, B. King, and D. Seipt, Extended locally constant field approximation for nonlinear Compton scattering, Phys. Rev. A **99**, 042121 (2019).

[95] A. Di Piazza, M. Tamburini, S. Meuren, and C. H. Keitel, Implementing nonlinear Compton scattering beyond the local-constant-field approximation, Phys. Rev. A **98**, 012134 (2018).

[96] C. N. Harvey, A. Ilderton, and B. King, Testing numerical implementations of strong-field electrodynamics, Phys. Rev. A **91**, 013822 (2015).

[97] A. Di Piazza, M. Tamburini, S. Meuren, and C. H. Keitel, Improved local-constant-field approximation for strong-field QED codes, Phys. Rev. A **99**, 022125 (2019).

[98] B. King, Uniform locally constant field approximation for photon-seeded pair production, Phys. Rev. A **101**, 042508 (2020).

[99] N. V. Elkina, A. M. Fedotov, I. Yu. Kostyukov, M. V. Legkov, N. B. Narozhny, E. N. Nerush, and H. Ruhl, QED cascades induced by circularly polarized laser fields, Phys. Rev. ST Accel. Beams **14**, 054401 (2011).

[100] C. P. Ridgers, J. G. Kirk, R. Duclous, T. G. Blackburn, C. S. Brady, K. Bennett, T. D. Arber, and A. R. Bell, Modelling gamma-ray photon emission and pair production in high-intensity laser–matter interactions, J. Comput. Phys. **260**, 273 (2014).

[101] A. Gonoskov, S. Bastrakov, E. Efimenko, A. Ilderton, M. Marklund, I. Meyerov, A. Muraviev, A. Sergeev, I. Surmin, and E. Wallin, Extended particle-in-cell schemes for physics in ultrastrong laser fields: Review and developments, Phys. Rev. E **92**, 023305 (2015).

[102] D. Del Sorbo, D. Seipt, T. G. Blackburn, A. G. R. Thomas, C. D. Murphy, J. G. Kirk, and C. P. Ridgers, Spin polarization of electrons by ultraintense lasers, Phys. Rev. A **96**, 043407 (2017).

[103] D. Del Sorbo, D. Seipt, A. G. R. Thomas, and C. P. Ridgers, Electron spin polarization in realistic trajectories around the magnetic node of two counter-propagating, circularly polarized, ultra-intense lasers, Plasma Phys. Controlled Fusion **60**, 064003 (2018).

[104] D. Seipt, D. Del Sorbo, C. P. Ridgers, and A. G. R. Thomas, Ultrafast polarization of an electron beam in an intense bichromatic laser field, Phys. Rev. A **100**, 061402(R) (2019).

[105] Y.-Y. Chen, P.-L. He, R. Shaisultanov, K. Z. Hatsagortsyan, and C. H. Keitel, Polarized Positron Beams Via Intense Two-Color Laser Pulses, Phys. Rev. Lett. **123**, 174801 (2019).

[106] Y.-F. Li, R. Shaisultanov, K. Z. Hatsagortsyan, F. Wan, C. H. Keitel, and J.-X. Li, Ultrarelativistic Electron-Beam Polarization in Single-Shot Interaction with an Ultraintense Laser Pulse, Phys. Rev. Lett. **122**, 154801 (2019).

[107] Y.-F. Li, R. Shaisultanov, Y.-Y. Chen, F. Wan, K. Z. Hatsagortsyan, C. H. Keitel, and J.-X. Li, Polarized Ultrashort Brilliant Multi-GeV γ Rays Via Single-Shot Laser-Electron Interaction, Phys. Rev. Lett. **124**, 014801 (2020).

[108] V. N. Baĭer, A. I. Mil'shteĭn, and V. M. Strakhovenko, Interaction between a photon and an intense electromagnetic wave, Sov. Phys. JETP **42**, 961 (1975).

[109] M. Marklund and P. K. Shukla, Nonlinear collective effects in photon-photon and photon-plasma interactions, Rev. Mod. Phys. **78**, 591 (2006).

[110] A. Di Piazza, C. Müller, K. Z. Hatsagortsyan, and C. H. Keitel, Extremely high-intensity laser interactions with fundamental quantum systems, Rev. Mod. Phys. **84**, 1177 (2012).

[111] B. King and T. Heinzl, Measuring vacuum polarization with high-power lasers, High Power Laser Sci. Eng. **4**, e5 (2016).

[112] V. Bargmann, L. Michel, and V. L. Telegdi, Precession of the Polarization of Particles Moving in a Homogeneous Electromagnetic Field, Phys. Rev. Lett. **2**, 435 (1959).

[113] C. Itzykson and Jean-Bernard Zuber, *Quantum Field Theory* (McGraw-Hill, New York, 1980).

[114] V. Shtabovenko, R. Mertig, and F. Orellana, New Developments in FeynCalc 9.0, Comput. Phys. Commun. **207**, 432 (2016).

[115] V. Shtabovenko, R. Mertig, and F. Orellana, FeynCalc 9.3: New features and improvements, Comput. Phys. Commun. **256**, 107478 (2020)

[116] V. Dinu, Exact final state integrals for strong field QED, Phys. Rev. A **87**, 052101 (2013).

[117] M. Boca and V. Florescu, Nonlinear Compton scattering with a laser pulse, Phys. Rev. A **80**, 053403 (2009).

[118] T. Heinzl, B. King, and A. J. Macleod, The locally monochromatic approximation to QED in intense laser fields, arXiv:2004.13035 [hep-ph] (2020).

[119] S. S. Bulanov, C. B. Schroeder, E. Esarey, and W. P. Leemans, Electromagnetic cascade in high-energy electron, positron, and photon interactions with intense laser pulses, Phys. Rev. A **87**, 062110 (2013).

[120] M. Tamburini and S. Meuren, Efficient high-energy photon production in the supercritical QED regime, arXiv:1912.07508 [hep-ph] (2019).

[121] A. Di Piazza, Completeness and orthonormality of the Volkov states and the Volkov propagator in configuration space, Phys. Rev. D **97**, 056028 (2018).

[122] D. J. Griffiths, *Introduction to Quantum Mechanics*, 1 ed. (Prentice-Hall, Upple Saddle River, New Jersey,1994).

[123] C. M. Bender and S. A. Orszag, *Advanced Mathematical Methods for Scientists and Engineers I* (Springer, New York, 1999).

[124] A. M. Fedotov, Conjecture of perturbative QED breakdown at $\alpha\chi^{2/3} \gtrsim 1$, J. Phys.: Conf. Ser. **826**, 012027 (2017).

[125] T. Podszus and A. Di Piazza, High-energy behavior of strong-field QED in an intense plane wave, Phys. Rev. D **99**, 076004 (2019).

[126] A. Ilderton, Note on the conjectured breakdown of QED perturbation theory in strong fields, Phys. Rev. D **99**, 085002 (2019).

[127] A. A. Mironov, S. Meuren, and A. M. Fedotov, Resummation of QED radiative corrections in a strong constant crossed field, Phys. Rev. D **102**, 053005 (2020).

[128] K. Ozaki, S. Takahashi, S. Aoki, K. Kamada, T. Kaneyama, R. Nakagawa, and H. Rokujo, Demonstration of polarization sensitivity of emulsion-based pair conversion telescope for cosmic gamma-ray polarimetry, Nucl. Instruments Methods Phys. Res. A **833**, 165 (2016).

[129] H. R. Band, G. Mitchell, R. Prepost, and T. Wright, A Møller polarimeter for high energy electron beams, Nucl. Instruments Methods Phys. Res. A **400**, 24 (1997).

[130] C. K. Sinclair, Electron beam polarimetry, in *The Eighth Beam Instrumentation Workshop*, edited by J. D. Masek and R. O. Hettel, AIP Conf. Proc. NO. 451 (AIP, New York, 1998), p. 23.

[131] A. Narayan, D. Jones, J. C. Cornejo, M. M. Dalton, W. Deconinck, D. Dutta, D. Gaskell, J. W. Martin, K. D. Paschke, V. Tvaskis *et al.*, Precision Electron-Beam Polarimetry at 1 GeV Using Diamond Microstrip Detectors, Phys. Rev. X **6**, 011013 (2016).

[132] D. P. Barber, H.-D. Bremer, M. Böge, R. Brinkmann, W. Brückner, Ch. Büscher, M. Chapman, K. Coulter, P. P. J. Delheij, M. Düren *et al.*, The HERA polarimeter and the first observation of electron spin polarization at HERA, Nucl. Instruments Methods Phys. Res. A **329**, 79 (1993).

[133] Y.-F. Li, R.-T. Guo, R. Shaisultanov, K. Z. Hatsagortsyan, and J.-X. Li, Electron Polarimetry with Nonlinear Compton Scattering, Phys. Rev. Appl. **12**, 014047 (2019).

[134] F. Wan, Y. Wang, R.-T. Guo, Y.-Y. Chen, R. Shaisultanov, Z.-F. Xu, K. Z Hatsagortsyan, C. H. Keitel, and J.-X. Li, High-energy gamma-photon polarization in nonlinear Breit-Wheeler pair production and gamma-polarimetry, Phys. Rev. Res. **2**, 032049(R) (2020).

[135] K. Aulenbacher, E. Chudakov, D. Gaskell, J. Grames, and K. D. Paschke, Precision electron beam polarimetry for next generation nuclear physics experiments, Int. J. Mod. Phys. E **27**, 1830004 (2018).

[136] T. G. Blackburn, D. Seipt, S. S. Bulanov, and M. Marklund, Radiation beaming in the quantum regime, Phys. Rev. A **101**, 012505 (2020).

[137] O. Valleé and M. Soares, *Airy Functions and Applications to Physics* (Imperial College Press, London, 2010).